Engineering Structures 267 (2022) 114674

Contents lists available at ScienceDirect

Engineering Structures

journal homepage: www.elsevier.com/locate/engstruct

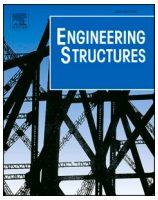

Spatial variability and stochastic finite element model of unreinforced masonry veneer wall system under Out-of-plane loading

Imrose B. Muhit [a,*], Mark J. Masia [b], Mark G. Stewart [b], Andrea C. Isfeld [b]

[a] School of Civil Engineering, University of Leeds, Woodhouse Lane, Leeds LS2 9JT, United Kingdom
[b] Centre for Infrastructure Performance and Reliability, The University of Newcastle, Callaghan, NSW 2308, Australia

ARTICLE INFO

Keywords:
Unreinforced masonry veneer wall
Spatial variability
Out-of-plane loading
Monte Carlo Simulation
Stochastic finite element analysis
Model error

ABSTRACT

Inconsistency in the quality of workmanship, the weather during construction, and materials may result in the high unit-to-unit spatial variability of mechanical properties in the same masonry structure. This paper develops a numerical modelling strategy and focuses on the stochastic assessment of unreinforced masonry (URM) veneer walls with spatially variable wall constituent material properties subjected to out-of-plane loading. 3-D finite element modelling of experimentally tested veneer walls was conducted using a micro-modelling approach combined with the Monte Carlo Simulation technique. Spatial stochastic finite element analysis considered the spatial variability of the properties of the wall components (mortar flexural tensile strength) and compared them with non-spatial analysis. The non-spatial analysis overestimates the wall system failure compared to spatial analysis, and the spatial analysis is considered to more realistically represent the variabilities of the URM veneer wall system. Sensitivity analysis is conducted to check the sensitivity of the veneer system behaviour to variability in the various input parameters. The variability of experimental results obtained in a parallel study are quantified and compared with stochastic finite element analysis (SFEA) results. The SFEA model developed in this study can estimate the behaviour and system peak load reasonably and are considered to be from the similar population as test results. Model errors are also included to assess the efficiency of the SFEA model.

1. Introduction

The masonry veneer wall is an external wythe of masonry connected to a backup system using wall ties, with various different types of ties being available. The backup systems, to which the masonry veneer walls are attached, range from non-loadbearing enclosure walls in reinforced concrete frames, through structural masonry or concrete walls, to light timber and steel stud frames. In Australia, the internal layer of the masonry veneer wall system is most often composed of timber framing and provides lateral support via wall ties attached to the external leaf of masonry. The Australian masonry structures design code AS3700 [1] has been in a limit states format since 1988. However, masonry design specifications have not been developed from reliability-based calibration methods but rather calibrated to past practice. Therefore, the actual level of safety of masonry structures is not known. The problem is compounded by the fact that the strength properties of masonry are highly variable, particularly the unit-to-unit flexural bond strength, due to variations in the quality of workmanship, the weather during construction, the difficulty of controlling site-batched mortar and the materials from location to location, all within one structure [2]. However, most of the existing analyses [3–8] of veneer wall systems assume homogenous material properties for flexural bond strength in the masonry wall, rather than considering the unit-to-unit spatial variability of flexural bond strength, the latter being a more realistic approach in examining material variability.

Unit-to-unit spatial variability refers to defining a unique strength parameter for each unit in the brick wall compared to its neighbouring units. This unit-to-unit variability can be considered as correlated to each other or fully independent. Variations of material properties can be incorporated into a numerical modelling study and the most popular method of realising this kind of modelling work is finite element analysis (FEA) combined with Monte-Carlo simulation (MCS). Baker [9] described the effects of random variation in joint strength and related this to the strength of walls spanning vertically. He carried out a Monte-Carlo simulation, checked the results against tests, and made predictions of the effects for different test procedures. Lawrence and Cao [10]

* Corresponding author.
E-mail addresses: i.muhit@leeds.ac.uk (I.B. Muhit), mark.masia@newcastle.edu.au (M.J. Masia), mark.stewart@newcastle.edu.au (M.G. Stewart), andrea.isfeld@newcastle.edu.au (A.C. Isfeld).

https://doi.org/10.1016/j.engstruct.2022.114674
Received 14 March 2022; Received in revised form 27 May 2022; Accepted 9 July 2022
Available online 17 July 2022

predicted the first cracking load for non-load bearing masonry walls under lateral loading using Monte Carlo simulations to take into account random variations of unit flexural bond strengths. Lawrence [11] determined the strength of masonry beams using similar MCS to those mentioned above, and several failure hypotheses, namely the weakest link hypothesis (leading to an estimate of strength based on the weakest single joint unit in each cross-section), and averaging hypothesis (leading to an estimate of strength based on averaging all joint units across each cross-section). These probabilistic analyses included beams spanning across the bed joints, beams spanning across perpends and wall panels supported on three or four sides. Stewart and Lawrence [12] modelled the unit-to-unit spatial variability in flexural bond strength during masonry reliability analyses for walls in vertical bending using MCS, using three idealised hypotheses, namely the weakest link, averaging and load redistribution hypotheses. They investigated the effect of wall width, workmanship and the discretising of masonry unit thickness on the reliability index.

Heffler [13] and Li et al. [14 –16] have made significant recent progress in understanding the influence of spatial variability of material properties on the bending strength of unreinforced masonry (URM) panels. Heffler [13] compared spatial and non-spatial FEA MCS results using the DIANA FEA software. The material input was established through validation of deterministic FEA using data from masonry panels previously tested by Doherty [17] in one-way flexure. A truncated normal distribution was used to represent bond strength with a mean value of 0.4 MPa, and coefficient of variation (COV) of 0.1, 0.3, and 0.5 for both spatial and non-spatial stochastic simulations. On the other hand, Li et al. [14 –16] used a simplified micro modelling strategy in DIANA FEA without considering the effect of bed joint thickness to predict the strength for non-load bearing single skin URM walls subject to one-way vertical bending, one-way horizontal bending, and two-way bending considering the unit-to-unit spatial variability of flexural tensile bond strengths, with and without correlation of adjacent unit strengths along each masonry course ($\rho = 0$, 0.4 and 1). They found $\rho = 0.4$ as the best-representing correlation between units. Using 3D nonlinear stochastic finite element analysis (SFEA), the probability distributions of wall strength were characterised. They also examined how spatial variability in unit flexural bond strength affects the variability of base cracking load, mid-height cracking load, peak load and behaviour of clay brick URM walls. Following a similar approach, Isfeld et al. [18] investigated the length effect for masonry walls under out-of-plane loading. The wall panel strength is shown to increase with length from one to four units, then stabilise with further length increase; however, the variability of the failure load significantly decreases with increasing wall length. They compared the output of MCS with the experimental results of Baker [19] and evaluated the model error (or model uncertainty). Vaculik and Griffith [20] developed a stochastic analysis method to calculate the ultimate strength of unreinforced masonry subjected to horizontal bending with combined failure modes. The tensile strengths of the mortar joints and brick units were considered as Weibull distributed random variables. Muller et al. [21] assessed the capacity and reliability of calcium silicate block walls of different dimensions subjected to eccentric axial load using SFEA. The unit-to-unit spatial correlation of the elastic modulus and compressive strength was varied between 0 and 1. The effect on load-bearing capacity was found to vary for walls of different sizes, with most showing an increase in load-bearing capacity with increasing spatial correlation. The importance of considering a realistic value for spatial correlation within spatial SFEA was demonstrated.

Nevertheless, none of these SFEA studies considered the veneer or cavity wall systems to estimate the failure load where unit-to-unit spatial variability for mortar and random variabilities for the material properties of wall ties and timber studs are considered. Moreover, SFEA modelling of masonry and masonry veneer systems is in its infancy, and there is still no suitable models developed for the model error of veneer system SFEA. This is due mainly to the lack of probabilistic information

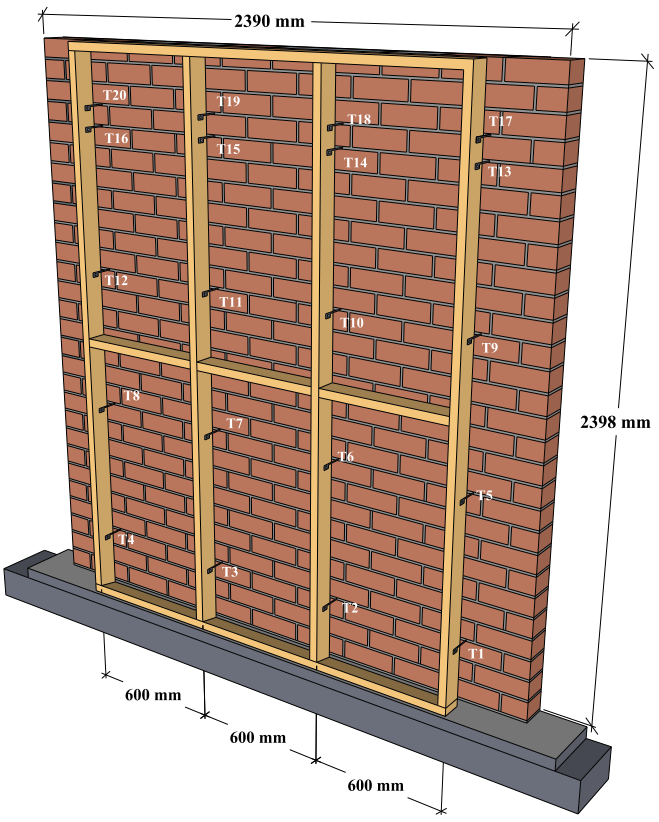

Fig. 1. Elevation of the full-sized URM veneer wall system [22]

for brick and mortar joint unit strengths, wall tie strengths and stiffnesses and unit-to-unit spatial variability. The computational and stochastic models developed in this study aims to build on the study of a single leaf masonry wall, to investigate the more complex behaviour associated with URM veneer and cavity wall systems.

In this study, an SFEA model is developed considering spatial variability of the wall component material properties to simulate the behaviour of the full-scale URM veneer wall system under out-of-plane loading. Spatial SFEA is compared with the non-spatial SFEA, and a sensitivity analysis evaluates the parameters' sensitivity for the SFEA model. Tie force history before and after veneer cracking are also reported to explain the veneer capacity and failure load. Finally, the SFEA results are compared with the experimental results of multiple testing of replicate walls, or Monte-Carlo experimental results conducted by Muhit et al. [22,23]. The model error is then calculated to check the model prediction efficiency and to assess the application of spatial SFEA in further reliability analyses.

2. Experimental testing programme

A total of 18 masonry veneer assemblies (see Fig. 1) of theoretically identical properties (geometry, type of masonry, wall ties, stress grade of timber stud, etc.) were tested by Muhit et al. [22,23] to determine the probabilistic behaviour of wall system collapse load. Among these identical 18 veneer walls, ten walls were tested in compression (inward loading on the wall surface and ties are in compression) and eight in tension (outward loading and ties are in tension) through lateral pressure loading. The dimensions of the wall assembly were 2398 mm (height) × 2390 mm (length) × 110 mm (thickness). The veneer wall assembly consists of a single leaf of a masonry wall and another leaf of timber studs, connected in between with five rows of ties, which typifies a portion of the wall system in a single-storey family home in Australia [24]. Extruded burnt clay brick units with a mixing ratio of mortar as

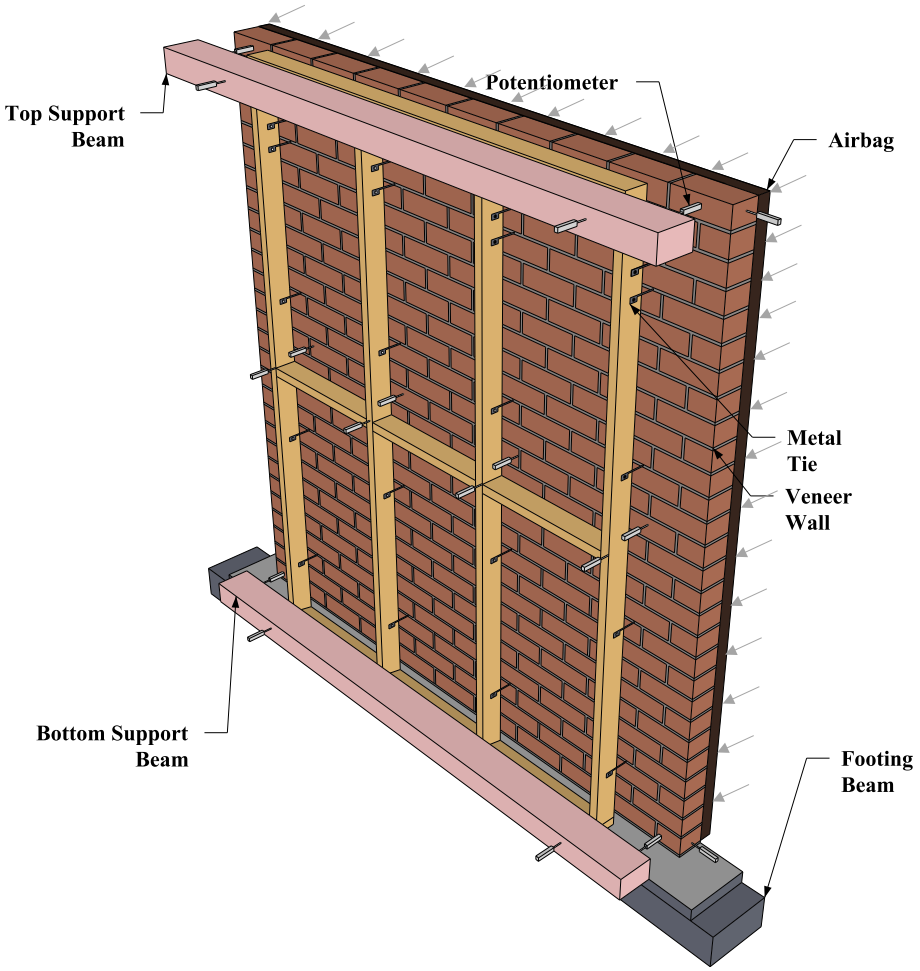

Fig. 2. Schematic view of the test setup for inward loading [22]

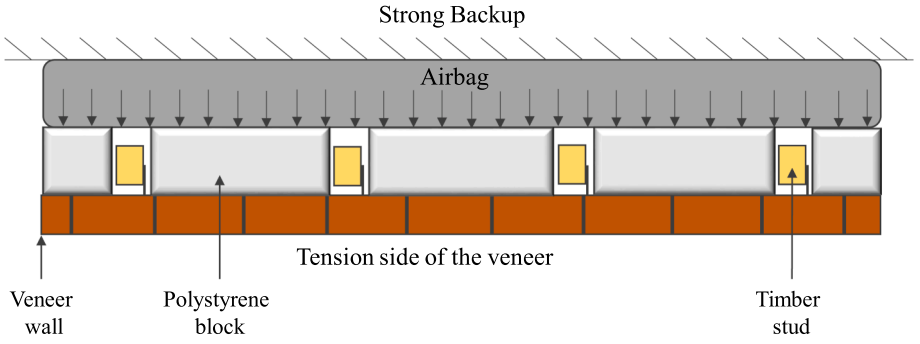

Fig. 3. Plan view of the test setup for outward loading [22]

1:1:6 (cement: lime: sand by volume) (Class M3) is used to construct the veneer wall specimens. The wall ties are side fixed to the timber studs with a nail to maintain a 50 mm cavity width. Machine-graded pine with a stress grade of MGP10 timber studs was used as a flexible structural backup. Along the full length of the base of the wall, a single membrane of damp-proof course (DPC) was installed.

Two inflatable airbags positioned within a closed loading frame generated evenly distributed lateral out-of-plane loading on the veneer wall. One wall specimen from each category (inward and outward loading) was tested under the semi-cyclic loading (increased in increments of 0.5 kPa) while the remaining specimens were tested for monotonic loading until the post-peak lateral pressure dropped by at least 20% of the peak load or failure (collapse) of the specimen. For the inward loading case, the lateral load was applied directly to the outer leaf of the masonry through the airbag system (Fig. 2). Top and bottom support beams were attached to the timber frame of the masonry veneer wall system (extended along the length of the wall) to provide lateral support. The outward loading setup intends that the veneer wall system would experience suction type loading. To achieve this, polystyrene blocks were placed between the airbag and the veneer wall to transfer airbag pressure to the veneer without touching the timber stud frame (Fig. 3). When the airbag is inflated, it starts to push the polystyrene blocks towards the veneer wall, and the ties of the veneer wall would be in tension. A parallel flange channel (PFC) steel beam extending along

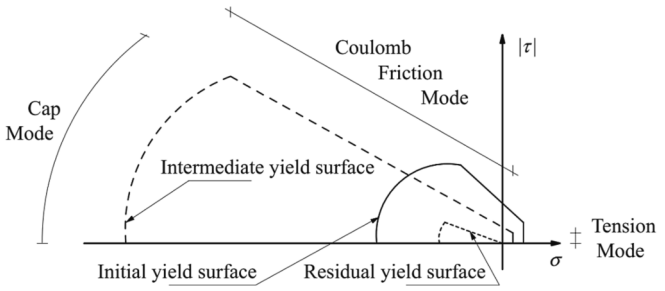

Fig. 4. Two-dimensional composite interface model [28]

the length of the wall was placed on the top of the timber studs and fastened with the testing rig to provide lateral support to the timber stud frame. Further details regarding the experimental testing program can be found in [22,23].

3. Finite element modelling

3.1. Veneer wall model

A deterministic three-dimensional (3-D) nonlinear finite element model for veneer wall was modelled using the commercial software package DIANA FEA 10.3 [25], which was selected for its ability to simulate a range of masonry behaviours. A simplified micro-modelling strategy [26,27] was adopted for the masonry modelling as it provides a computationally efficient method of accurately representing the behaviour of URM walls subjected to one-way flexure [13–16,18]. The rationale for this choice is that not only is the micro-model capable of reproducing crack patterns and the complete load–displacement path of a masonry structure, but also it allows consideration of the unit to unit variability in the spatial stochastic analyses. In simplified micro-modelling, units are represented by linear elastic continuum elements and the behaviour of the mortar joints and the unit/mortar interface is lumped into discontinuum elements. As the mortar joint and the mortar/brick unit interface are lumped into a zero-thickness interface element, the brick units were modelled as 3-D solid expanded units (HE20 CHX60) to incorporate mortar-joint thickness. The individual brick units were modelled as two halves and potential crack planes were modelled using an interface at the mid-length of each brick. Potential brick crack interface and mortar joints were modelled as a linear softening model and a combined cracking-shearing-crushing model [27,28], respectively. The combined cracking-shearing-crushing model can simulate a tensile and shear failure, frictional slip and crushing along the material interfaces. A two-dimensional composite interface model is based on multi-surface plasticity, illustrated in Fig. 4, which includes the tension cut-off model to describe the joint cracking failure, the Coulomb-friction model to depict the sliding shear failure and the elliptical cap model to explain the masonry compression as well as the diagonal cracking of the brick unit. The two-dimensional interface model is extended to a three-dimensional model, which enables the description of the delamination (tension cut-off) and relative shear-slipping of two planes (Coulomb friction). However, the two-dimensional tension criterion remains unchanged, and no three-dimensional compression cap is implemented in DIANA FEA 10.3 [25]

Typically, the nonlinear behaviour of wall ties can be modelled as ideal elastic–plastic behaviour with or without kinematic and isotropic hardening. However, the behaviours of wall ties under compression and tension were found to differ (in the experimental investigations of wall ties [23,29]) from the ideal elastic–plastic model, as will be discussed later. Considering these conditions, DIANA FEA has two options to incorporate (a) monotonic structural nonlinear analysis and (b) cyclic/dynamic structural nonlinear analysis. Cyclic/dynamic analysis considers the 'Modified two-surface model', which is the plasticity model for cyclic/dynamic structural steel analysis. In contrast, to incorporate material behaviour under monotonic loading (case of the current study), two constitutive models are available in DIANA FEA, (i) the Nonlinear elasticity material model and (ii) the Total strain crack model. When unloading–reloading effects are negligible, the nonlinear elasticity model is the preferred option for this study. Therefore, to incorporate material behaviour under monotonic loading the nonlinear elasticity material model with user-defined stress–strain diagram model (EPSSIG diagram) was selected to define the nonlinearity of the wall ties for this study. The wall ties were modelled as enhanced 3-D 3-noded truss elements (CL9TR), similar to the regular truss elements with the additional ability to curve. Wall ties are perfectly connected to the masonry in the FEA and the nonlinear behaviour of the masonry-tie and the tie-timber interfaces are modelled via the tie nonlinear stress–strain behaviour.

The veneer wall backup frame (timber studs) was considered as a 3-D solid element with a linear elastic material in the FEA as no timber studs were cracked (reached beyond the elastic limit) during any of the full-scale veneer wall tests.

Therefore, a single leaf non-loadbearing veneer wall of dimensions 2400 mm (height) × 2400 mm (width) × 110 mm (thickness) was generated in DIANA FEA GUI, to replicate the tested walls. The first row of ties was at 300 mm from the bottom of the wall; therefore, four vertical lines of ties (with timber frame) were spaced at 600 mm in the horizontal and vertical direction, as per the tested veneer wall system setup [22]. The timber frame members had a cross-section of 90 mm × 35 mm, and the centre to centre distance is 600 mm. Each wall tie is 8.25 mm^2 in cross-sectional area (dimension measured from the actual tie used) and side fixed from masonry wall to timber studs with 50 mm cavity width.

Table 1
Summary of the FEA model element and mesh type.

Material	Element	Mesh Size
Half Brick Unit	HE20 CHX60	2 × 4 × 1
Mortar Joint	IS88 CQ48I	2 × 4 × 1
Crack Interface	IS88 CQ48I	1 × 4 × 1
Wall Tie	CL6TR	2 elements
Timber Stud	HE20 CHX60	2 × 2 × variable

3.2. Mesh refinement study

A mesh refinement study was completed for a deterministic 3-D model, and 2 × 4 × 1 mesh density for the half brick unit satisfied the requirements of accuracy and computation time, i.e., four elements through the wall thickness, two elements along the length and one element over the height. This is in agreement with the mesh densities used by Li et al. [14] and Isfeld et al. [18]. As the ties were modelled as truss elements, two elements along the length of each tie were considered, which is sufficient to evaluate tie force and tie buckling across the cavity. The timber studs were meshed with two elements along with the thickness and length (cross-section dimensions), and meshing along the height was done to match with tie position and nodes. The summary of the mesh density for masonry, wall ties and timber are shown in Table 1. The self-weight of the masonry veneer wall system's components (masonry, ties and timber studs), i.e., gravity loadings were considered in the model.

3.3. Loading and boundary conditions

The boundary conditions for the FEA model were established according to the experimental setup (full-scale veneer wall tests) to simulate the testing methodology. To represent the inward loading (ties are in compression), quasi-static uniform pressure loading was applied on the wall's exterior skin throughout the wall, whereas pressure was applied in the opposite direction (suction pressure) to represent the

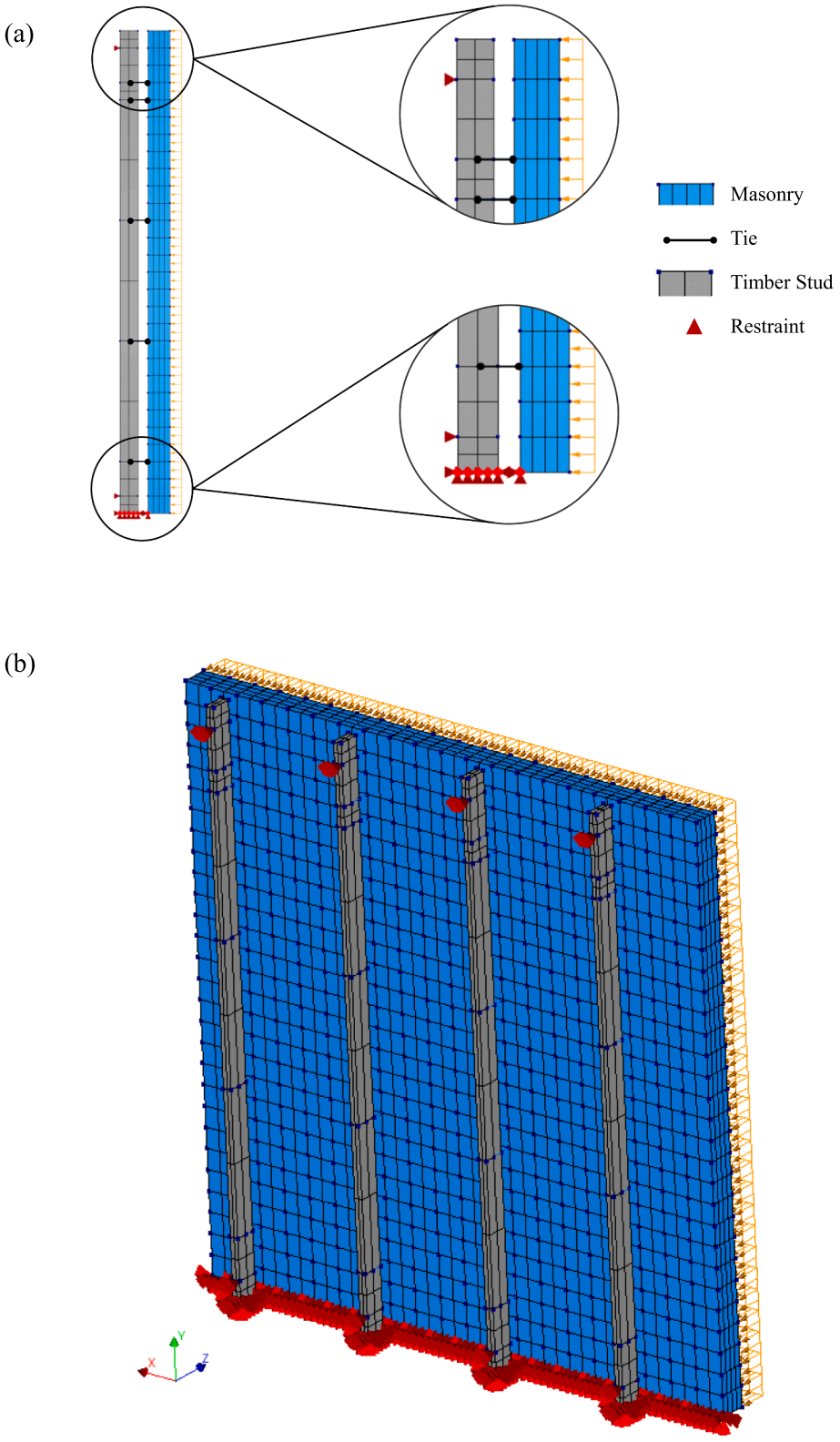

Fig. 5. (a) Side view and (b) isometric view of the veneer wall system FEA model (inward loading).

outward loading (ties are in tension).

3.3.1. *Inward loading*

During the experimental program, it was observed that the interface between the masonry veneer and the footing beam (which includes the damp proof course) opened in a flexural mode, with the wall rotating about the edge adjacent to the cavity. Out-of-plane movement (sliding) was not observed in any of the tests. To simulate this unique support condition, instead of bonding the bottom course and/or surface of the wall to the underlying footing, one edge of the wall (first-course unit),

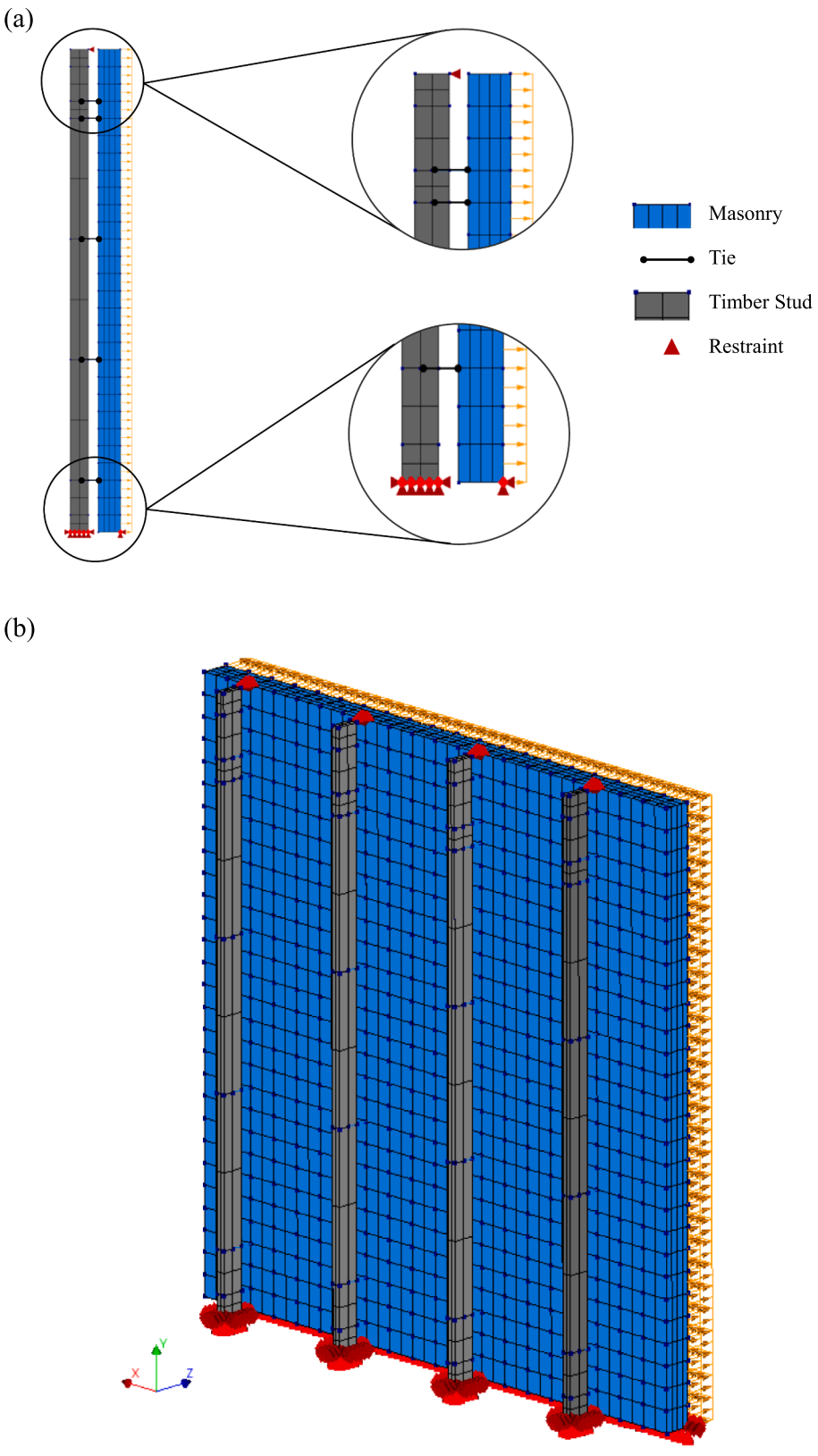

Fig. 6. (a) Side view and (b) isometric view of the veneer wall system FEA model (outward loading).

adjacent to the cavity, was restrained against translation for all directions as shown in Fig. 5. Moreover, no mortar interface was considered below the first course units in order to achieve the expected veneer wall system behaviour. The veneer wall model has no support at the top edge and was attached to timber studs via five rows of wall ties. Out-of-plane restraint (roller support) was introduced at the top and bottom of the timber studs, at one brick high distance from the extreme ends, to represent the exact position of the lateral support provided during wall

Table 2
FEA input of masonry material parameters.

Parameter	Mean	COV	Unit	Data Source
Brick Unit				
Elastic Modulus	25,500	–	N/mm^2	Muhit et al. [22]
Poisson's ratio	0.15	–		Assumed
Density	1.8 × 10^{-9}	–	T/mm^3	Assumed
Brick Crack				
Linear Normal Stiffness Modulus	1000	–	N/mm^3	Heffler [13]
Linear Shear Stiffness Modulus	1000	–	N/mm^3	Heffler [13]
Direct Tensile Strength	1.28	–	N/mm^2	Muhit et al. [22]
Fracture Energy	0.037	–	Nmm/mm^2	Lourenco [30]
Mortar Joint (Combined cracking-shearing-crushing)				
Linear Normal Stiffness	471	–	N/mm^3	Muhit et al. [22]
Liner Shear Stiffness	196	–	N/mm^3	Muhit et al. [22]
Flexural Tensile Strength [Inward loading]*	0.40	0.42 (Lognormal)	N/mm^2	Muhit et al. [22]
Flexural Tensile Strength [Outward loading]*	0.42	0.47 (Lognormal)	N/mm^2	Muhit et al. [22]
Ratio of Flexural Tensile Strength to Direct Tensile Strength*	1.5	0.132 (Lognormal)	–	Gooch et al. [33]
Tensile Fracture Energy [Inward loading]**	0.00473	see Eqn. (1)	Nmm/mm^2	Heffler [13]
Tensile Fracture Energy [Outward loading]**	0.00488	see Eqn. (1)	Nmm/mm^2	Heffler [13]
Cohesion (shearing)**	0.38	see Eqn. (2)	N/mm^2	Muhit et al. [22]
Friction Angle (shearing)	0.39	–	–	Muhit et al. [22]
Dilatancy Angle (shearing)	0.55	–	–	Petersen [32]
Residual Friction Angle (shearing)	0.39	–	–	Assumed
Confining Normal Stress (shearing)	−1.0	–	N/mm^2	Petersen [32]
Exponential Degradation Coefficient (shearing)	1.9	–	–	Petersen [32]
Masonry Compressive Strength (crushing)**	25.2	see Eqn. (3)	N/mm^2	Muhit et al. [22]
Compressive Fracture Energy**	23.56	see Eqn. (4)	Nmm/mm^2	Lourenco [30]
Shear Traction Control Factor C_s (crushing)	9.0	–	–	Lourenco [26]
Equivalent Plastic Relative Displacement	0.013	–	–	Muhit et al. [22]
Mode-II Fracture Energy Factor, a	−0.8	–	–	Petersen [32]
Mode-II Fracture Energy Factor, b	0.05	–	–	Petersen [32]

*Spatially variable
**Fully correlated spatial variable

tests. The bottom surface of the timber frame was restrained completely for any movements to replicate the bolted connection of the timber frame with the footing.

3.3.2. Outward loading

In the experimental tests, the bottom bed-joint (the connection between the first course of bricks and DPC) edge closest to the studs was cracked and opened due to the bending of the brick veneer wall under outward lateral pressure. Hence, the outer edge (tension side) of the wall was restrained in all directions (pin support), while the edge adjacent to the cavity is kept free (see Fig. 6). To achieve the expected veneer system behaviour, no mortar interface was considered beneath the first course of units. Moreover, the brick veneer wall top edge has no support, i.e., the veneer was supported by timber studs at different courses via wall ties. The bottom of the timber studs was restrained for all directions and the top edge of the timber, closest to the cavity, was supported for lateral direction (roller support), which replicates the support condition (PFC as timber top support) of the experimental wall tests. No rotations were restrained for any support throughout the veneer wall system.

3.4. Probabilistic material properties of SFEA

In a simplified micro-model, DIANA FEA requires as input a series of unique material properties to define the masonry, ties, and timber studs. The material parameters used as input for the FEA model were obtained from the material characterisation testing conducted during the veneer wall testing program described in [22], [23] and [29]. The masonry prism compression test, triplet shear test and the bond wrench test were conducted to probabilistically define the material properties in the mortar joint interface elements. To measure the flexural tensile strength of the brick to mortar bond, bond wrench testing was conducted for every batch of the mortar used to build the walls. Similarly, the modulus of rupture test was used to measure the flexural tensile strength of the bricks and hence to define the tensile strength of the potential brick crack interface elements. High interface stiffness values of the potential brick crack elements were set to maintain the continuity of brick displacements across the interface. Other parameters for masonry were taken from the literature and are shown in Table 2. To distinguish between inward (ties in compression) and outward (ties in tension) loading scenarios and to make a logical comparison with the experimental results, FEA input sources for a specific loading scenario is restricted to the experimental data obtained from that particular loading type.

It is necessary to quantify and restrict the number of random variables to only those parameters on which the veneer wall system response under one-way vertical bending is sensitive. Random variables can be categorised as statistically independent ($\rho = 0$), spatially variable, and/or spatially dependent which are fully correlated to a spatially variable property. These characterisations are identified in Table 2 and the remaining properties are represented with mean values (deterministic values) because changes of these parameters have a negligible effect on the overall system behaviour subjected to vertical bending. As masonry is much stiffer than the flexible backup (timber frame), variation of elastic modulus of brick or masonry has less sensitivity in bending and overall system peak load. For URM in one way bending Isfeld et al. [18] found that doubling or halving the Young's Modulus resulted in an increase or decrease of the failure load by approximately 5%, this is expected to be reduced in the case of veneer walls as the brick is much stiffer than the timber framing. Similarly, Heffler [13] found the shear properties including cohesion, friction angle, shear fracture energy, confining normal stress and dilatancy to have minimal effect on the failure load URM in one-way vertical bending. Nevertheless, the flexural tensile strength and associated fracture energy of the mortar joint, wall tie strength and stiffness, and timber stud stiffness predominantly govern the behaviour and failure of the veneer wall system under out-of-plane loading; thus, the material properties of these parameters were treated as a probabilistically variable in the FE model.

3.4.1 Flexural and direct tensile strengths of the masonry

Flexural tensile strengths (f_{mt}) of the masonry were obtained from bond wrench tests conducted for each batch of mortar for each wall and used to determine the direct tensile strength (f_t) required as input in DIANA FEA. In several studies [13–16,18] f_{mt} is divided by 1.5 to obtain f_t, based on the work of Van der Pluijm [31]. Van der Pluijm [31] discussed this relationship but does not present a large enough sample of data to produce a meaningful estimation of the variability of this ratio for mortar joints. The consideration of variability of the ratio 1.5 is not well documented in the literature; however, Gooch et al. [33] adopted

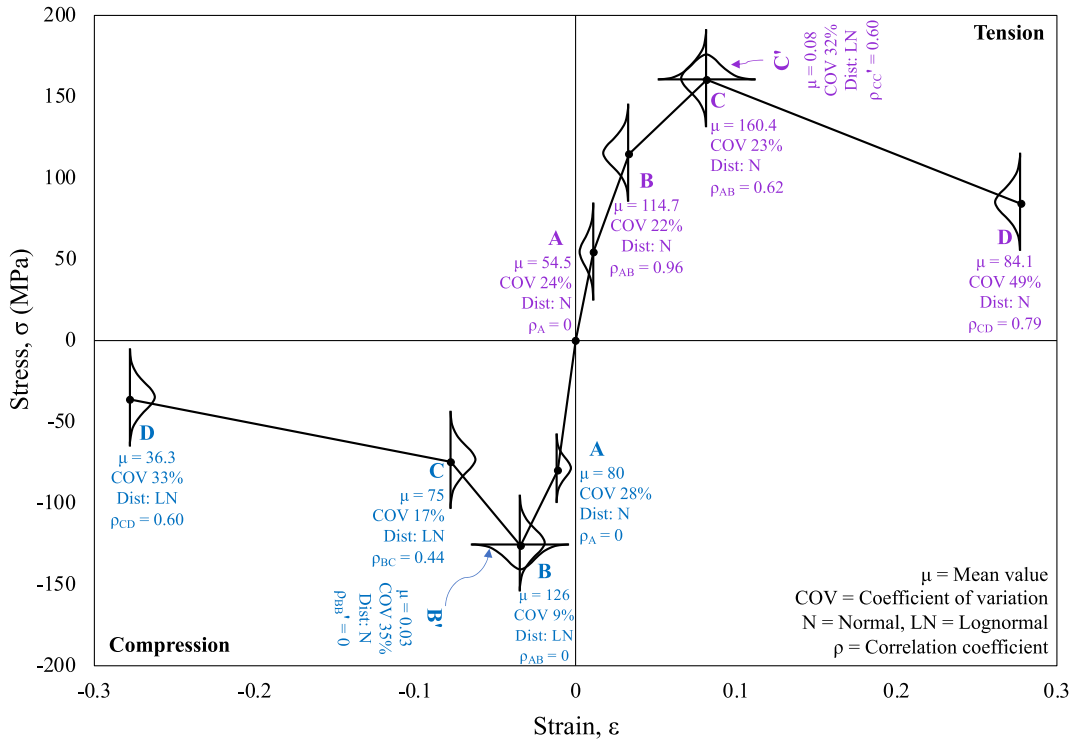

Fig. 7. Summary of tie constitutive law input for SFEA.

the distribution and variability of the model (where the ratio of 1.5 was considered as a variable) based on the conclusions made by Raphael [34]. In this study, the flexural to direct tensile strength ratio is considered as a variable (a mean of 1.5 with a COV of 0.132, and lognormal distribution) similar to Gooch et al. [33]. Probabilistic material properties of flexural and direct tensile strengths are shown in Table 2.

3.4.2 Tensile Fracture Energy

Tensile fracture energy (G_f^I) was not measured directly; hence, it was considered as a fully correlated variable to direct tensile strength (f_t) for the mortar joints in the SFEA [13], expressed as:

$$G_f^I = 0.01571 f_t + 0.0004882 \tag{1}$$

3.4.3 Cohesion

Although cohesion was determined from the shear triplet test [23], a representative mean value may not be suitable to satisfy the requirements of composite interface model criterion [28] (see Fig. 4) during the spatial SFEA. Masia et al. [35] demonstrated that the cohesion of masonry is correlated to the flexural tensile strength of mortar joints, and the relationship can be established by bond wrench tests and triplet tests. However, Milani and Lourenco [36] outlined the following relationship between direct tensile strength and cohesion:

$$c = 1.4 f_t \tag{2}$$

Therefore, cohesion is considered fully correlated with direct tensile strength (f_t) for SFEA in accordance with equation (2). The consideration of the 1.4 factor between cohesion and tensile strength may introduce a modelling error; however, Li et al. [15] suggested that consideration of model error statistics related to cohesion is a governing parameter for masonry walls in horizontal bending whereas for vertical bending (which is the current study case) the wall is not susceptible to shear and slip failure. Moreover, from the full-scale wall tests [22,23] no evidence of shear failure was observed; therefore, the inclusion of fully correlated cohesion is considered to be sufficient for the current study.

3.4.4 Masonry compressive strength

The use of a single fixed value (25.2 MPa from testing) for compressive strength of masonry $(f_m^{'})$ is not appropriate for all corresponding tensile strength values. In the DIANA FEA software, the nonlinear behaviour of a brick–mortar joint is defined by the composite interface model, where compressive strength followed the elliptical cap model (compression cap model) and is related to the tension cut-off model. Therefore, it is essential to change the compressive strength with the change of tensile strength, especially for higher tensile strengths. In this SFEA, when the direct tensile strength (f_t) is more than the mean value (0.27 MPa), f_t is multiplied by a 'factor' to increase the compressive strength accordingly and conform to the compression cap model. The factor was chosen based on the ratio of mean compressive strength (25.2 MPa from testing) to mean direct tensile strength (0.27 MPa from testing). The following relationship is used to ensure incremental masonry compressive strength throughout the SFEA:

$$f_m^{'} = \frac{25.2}{0.27} f_t = 93.33 f_t \tag{3}$$

Hence, the compressive strength of masonry is a dependent variable and assumed to be fully correlated to direct tensile strength. Moreover, the compressive fracture energy is another dependent variable to compressive strength, which is calculated from the relationship given by Lourenco [30]:

$$G_c = 15 + 0.43 f_m^{'} - 0.0036 \left(f_m^{'}\right)^2 \tag{4}$$

3.4.5 Wall tie strengths and displacements

Probabilistic material properties of wall ties are obtained from the probabilistic characterisation of masonry veneer wall ties described in [23,29]. DIANA FEA needs as input a stress–strain relationship in the

Table 3
Statistical elastic modulus input for timber studs [22]

Specimen Type	Mean (MPa)	COV	Distribution
Inward loading	10,275	0.18	Gamma
Outward loading	12,479	0.26	Lognormal

form of user-supplied data; hence, the tie-constitutive law (as to load–displacement) is converted to the stress–strain curve (see Fig. 7) and was included in this SFEA. While this relationship is from the mean values, probabilistic properties (including correlations between some points) were input in the SFEA according to the statistical parameters shown in Fig. 7 for characteristic points of this tie-constitutive law. The mean elastic modulus of the wall ties under tension and compression are considered as 4898 MPa (with a COV of 0.24) and 7190 MPa (with a COV of 0.28), respectively.

3.4.6 Timber stud stiffness

The probabilistic elastic modulus and bending strength of the timber studs used in the wall tests were evaluated in the timber characterisation tests [22,23]. As timber studs were not loaded up to the bending strength point (failed) during wall tests, all the timber studs were modelled as linear elastic in the SFEA; therefore, the elastic modulus is the only variable material property for the timber studs. Gamma and lognormal distributions from timber characterisation tests appeared to be the best fit for inward and outward loading timber samples, respectively. The properties of the timber studs used in the SFEA model are shown in Table 3.

3.5. Spatial SFEA

Heffler [13] investigated the spatial distribution of flexural tensile strength along the length and over the height of series of unreinforced masonry walls. It was found that correlation from one course to the next over the height of the wall was negligible, but that weak correlation did exist from one unit to the next along a masonry course at a given height. Three possible scenarios can be assumed to account for variability in wall bond strength (flexural tensile strength, cohesion and tensile fracture energy), tie and timber strength parameters, (a) fully correlated random variables ($\rho = 1.0$), (b) statistically independent variables ($\rho = 0.0$) and (c) defined correlation ($0 < \rho < 1$). For a fully correlated case, parameters would be varied for each simulation but consistent for each location in the wall, i.e., non-spatial analysis. However, for the statistically independent scenario, parameters are randomly varied at each location of the wall. In the spatial SFEA, a spatial correlation of mortar joint $\rho = 0.4$, established by Heffler [13], was assumed to occur within courses of masonry, and no correlation (statistical independence) was assumed between masonry courses and perpend joints. Correa et al. [37] showed that the mean correlation between courses is<0.2, which indicates a weak correlation. In addition, non-spatial analysis and spatial analysis with $\rho = 0$ is also considered to evaluate the effectiveness of spatial variability consideration of mortar joint tensile strength in SFEA. For wall ties, material properties were randomly distributed without any consideration of spatial correlation, i.e., statistically independent. To avoid the negative stresses or stiffnesses, stresses are truncated at 0.01 MPa (generate positive strength value) for the normal distribution, and $0.033 < \varepsilon_C^T < 0.278$ and $0.011 < \varepsilon_B^C < 0.078$ were introduced, where ε_C^T and ε_B^C represent strains at point C under tension and at point B under compression, respectively.

In order to automate the whole procedure, a programming code in MATLAB [38] was written to randomly generate and spatially assign the strength based on correlation. To write the DIANA FEA input, a python script (.py file) was generated from MATLAB [38], which incorporates all the commands for DIANA FEA, and then the scripts were run in batches for Monte-Carlo simulations (MCS).

3.6. Analysis procedure

To simulate material softening and unloading, a nonlinear structural FEA approach was adopted. Moreover, the DIANA FEA default integration scheme is used as it is appropriate for most types of meshes and analyses. Automatic incrementation with the arc length control method (incremental-iterative solution and indirect displacement control) was used to capture the load–displacement behaviour along with the range of possible results in FEA. This is done by simultaneously adapting the size of the increment, i.e., the applied force is increased proportionally to the change in the load-factor, which varies in every iteration to facilitate convergence. The modified Newton-Raphson method with simultaneous force and displacement convergence norms (Euclidian norm) was chosen to determine the displacement vector's iterative increment. With this approach, a linear approximation of the stiffness matrix is used for the first tangent at each iteration. The maximum

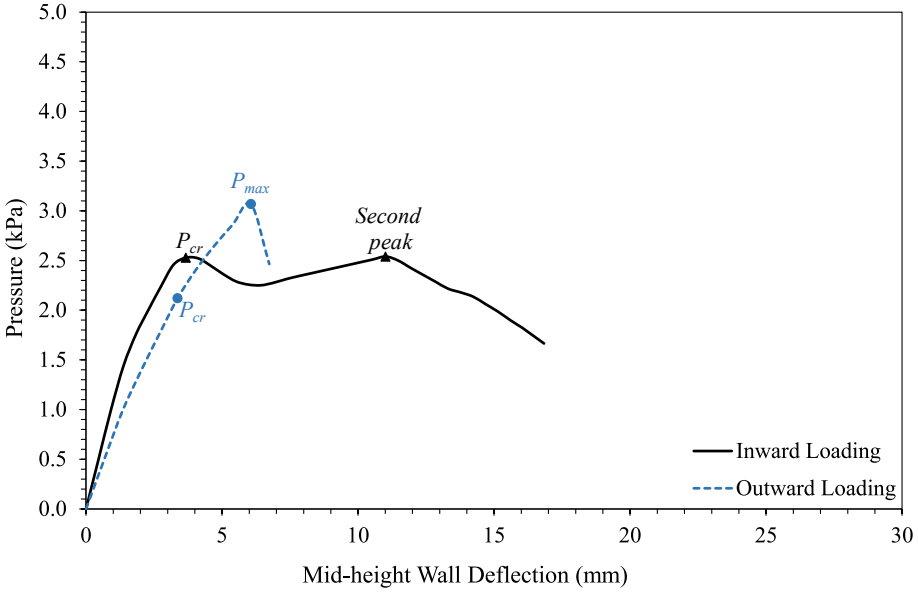

Fig. 8. Pressure vs mid-height wall displacement history of deterministic FEA for inward and outward loading.

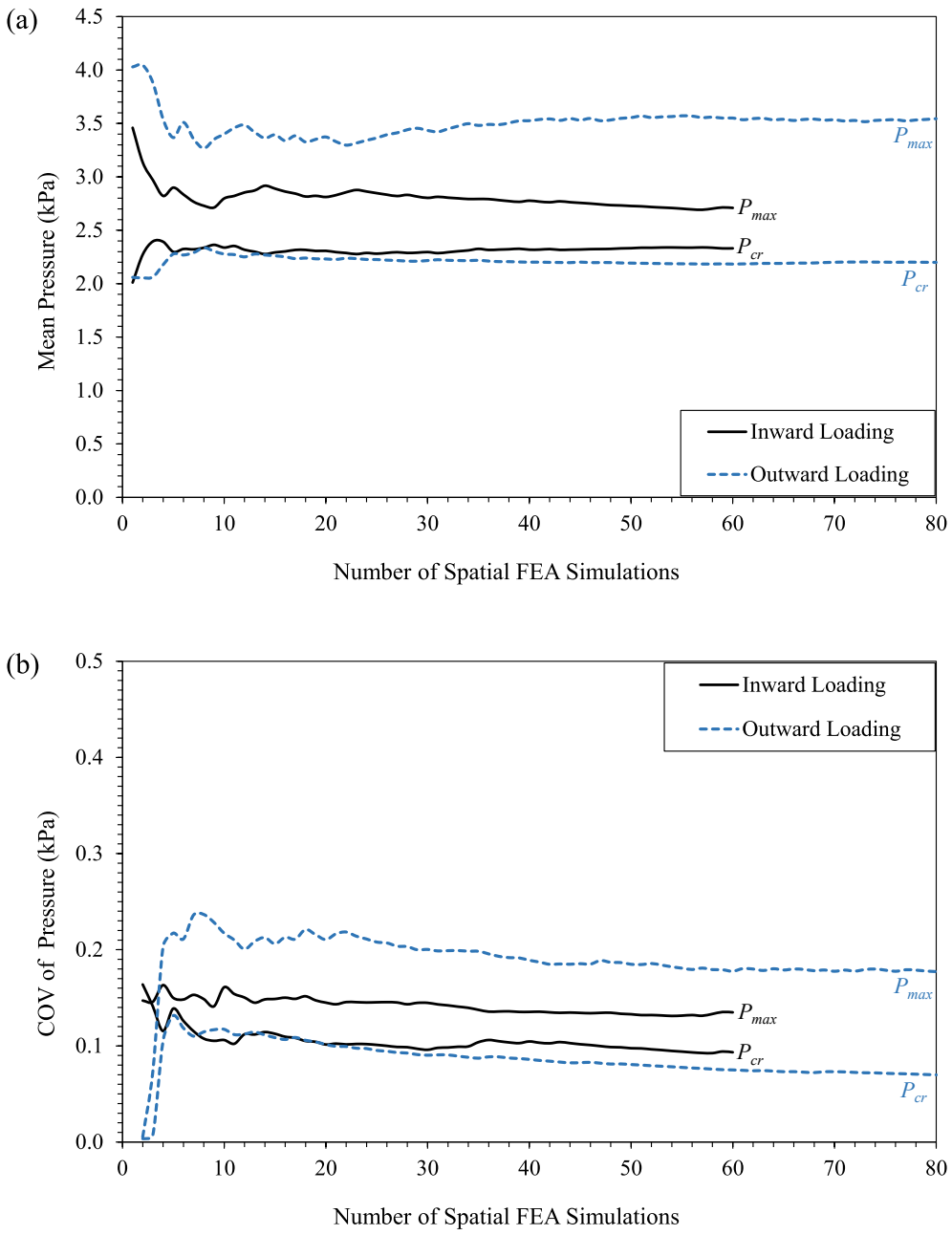

Fig. 9. Convergence of (a) mean and (b) COV of masonry cracking and system peak load for inward and outward loading.

number of steps and iterations were selected so that behaviour beyond the peak system load can be captured and terminated before complete unloading to minimise the CPU time.

4. Results and discussion

4.1. Deterministic FEA

For inward loading, the brick veneer cracks at 2.53 kPa (P_{cr}), which is significantly higher than the mean veneer cracking load for the experimental wall tests of 1.74 kPa [22,23]. One reason for the disparity could be that deterministic FEA considers all the mortar joints as homogenous, with flexural strength equal to the mean value. However, in the experimental wall tests, the presence of weaker than average joints could initiate failure at stresses lower than the mean strength. The second peak in the deterministic FEA is less than the veneer cracking load (P_{cr}), which results in P_{cr} being the veneer system peak load (P_{max}) for the FEA simulation (see Fig. 8). This might be because when the veneer cracks at a lower pressure load (as in the experiments), the wall ties are relatively undamaged; hence, the veneer wall system has the capacity to absorb more pressure until almost all ties reach their yielding point. By contrast, in the FEA model, with higher pressure being reached prior to veneer cracking, some of the ties may already be damaged and hence less able to play a role in load sharing post veneer cracking, leading to a lower peak load for the veneer wall system. The typical failure mode at masonry veneer cracking load (P_{cr}) for the deterministic FEA model is a few horizontal cracks (on the wall face closest to the timber studs) at the mid-height region throughout the wall length.

For outward loading, it is ambiguous to understand whether the veneer cracked before the peak load (3.06 kPa) as there is no pressure drop (see Fig. 8); therefore, based on the change of stiffness (in the load–deflection response) and substantial interface relative displacement, veneer cracking point (P_{cr}) is determined as 2.12 kPa. This estimated P_{cr} from the outward deterministic FEA model is higher than the

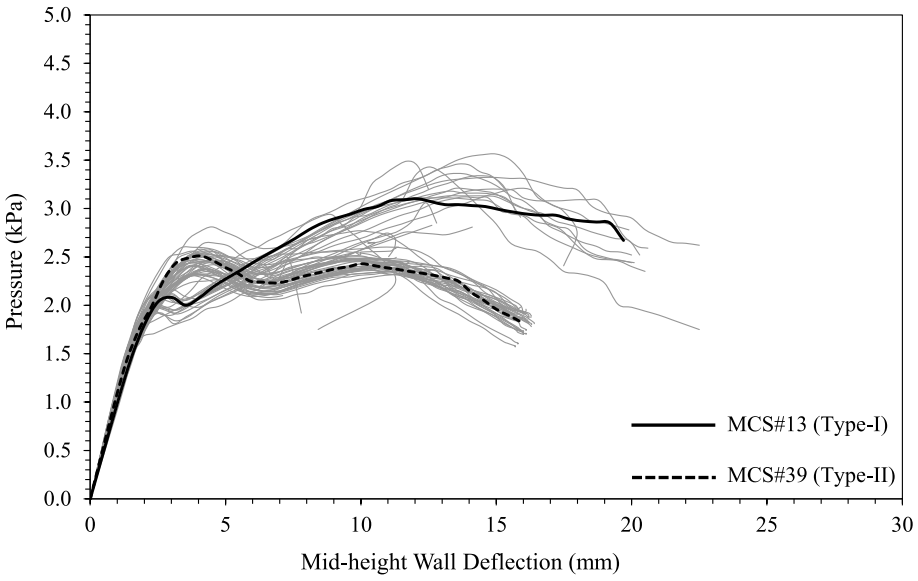

Fig. 10. Pressure load vs deflection plots for 60 MC realisations under inward loading (spatial analysis, $\rho = 0.4$).

load observed from wall tests.

4.2. Stochastic FEA convergence

It is essential to understand that the veneer cracking load (P_{cr}) is an intermediate load where the purpose of this study (from the design point of view) is to capture the system peak load (P_{max}), making this FE model effective. A convergence check (for spatial simulations with $\rho = 0.4$) on the mean and COV of failure loads (veneer cracking and system peak load) were performed as a means of stabilisation of the mean and COV to assess the number of simulations required.

Fig. 9 shows the stabilisation of mean masonry cracking and system peak load and corresponding COV for out-of-plane inward and outward loading. It is evident that 60 FE simulations for the inward loading scenario (VWI) and 80 simulations for the outward loading scenario (VWO) can be deemed as sufficient number to capture the fluctuation of the cracking and system peak load. Similar checks were provided for non-spatial stochastic simulations ($\rho = 1.0$) and spatial simulations with $\rho = 0$. More efficient MCS methods, such as LHS may be suitable for improving the rate of convergence as used by Milani and Benasciutti [39].

4.3. Spatial analysis with $\rho = 0.4$

4.3.1. Inward loading

Fig. 10 represents the pressure vs mid-height wall deflection outcomes of 60 MCS runs under inward loading. The mean and COV of P_{cr} is 2.33 kPa and 0.09 whereas for P_{max} it is 2.71 kPa and 0.13, respectively. Two distinct types of load–displacement behaviour are evident, those with a higher second-peak than veneer cracking load (Type-I), and the remaining are with an equal or lower second peak than the first peak (veneer cracking load) (Type-II). If the second peak is higher than the first peak (masonry veneer cracking load, P_{cr}), the second peak is considered as veneer system peak load (P_{max}), else the first peak is considered as both P_{cr} and P_{max}. Type-II failures merely depend on masonry strength, while Type-I failures are the combination of masonry strength and tie strength, which involves higher degrees of variability.

To examine the two distinctive load–displacement behaviours of spatial SFEA, two representative simulations (two individual realisations) were chosen, MCS#13 and MCS#39, as Type-I (second-peak $>$ P_{cr}) and Type-II (second-peak $\leq P_{cr}$) representative samples, respectively (shown in Fig. 10). MCS#13 and MCS#39 are referred to as Type-I and Type-II onwards in this paper.

Figs. 11 and 12 show the distributions of tensile strengths and veneer cracking patterns for the representative Type-I and Type-II behaviours at P_{cr} and P_{max}. For Type-II, the veneer cracked at a higher pressure load, crack widths are significantly narrower compared to the Type-I, where the veneer cracked at a lower pressure level (see Fig. 11). Also, higher tensile strength joints (darker shade) are predominant in the mid-height zone for Type-II (see Fig. 11 (b)), causing the veneer to crack at a comparatively higher load. Although cracks are distributed throughout, the crack width is not uniform in a particular course due to unit to unit bond strength variability. A majority of the mid-height cracks are between 0.07 mm and 0.1 mm for Type-I, whereas mid-height cracks are$<$0.03 mm for Type-II. The cracking pattern at P_{max} is shown in Fig. 12, and it is noted that for Type-II, $P_{cr} = P_{max}$ as the second peak is less than or equal to the first peak (P_{cr}). However, cracking width at the second peak for Type-II was analysed and found a negligible increase ($<$0.01 mm) from P_{cr}. On the contrary, a significant increase in crack widths is observed for the Type-I sample at P_{max}.

Axial force in the ties is considered as the crucial parameter to understand the stress level, yielding (buckling), post-buckling and force redistribution among the wall ties, which explains why the second peak of the veneer load–displacement plot could or could not surpass the first peak. For a deterministic model, tie forces at a particular row for a given loading step are almost equal due to the equal deflection of the tie-timber connection (which is related to the timber stiffness). In contrast, tie forces at a specific row fluctuate notably in SFEA due to varying timber stiffness, which results unsymmetric deflections between timber studs. As tie strengths and stiffnesses are also randomly generated throughout the veneer wall, tie failure (yielding/buckling) is not expected to co-occur in a specific row. The random failure of ties in SFEA coincides with the failure pattern observed from the wall testing. As tie strengths vary spatially for all twenty ties and yielding would occur at different stress levels, it is essential to show the tie strengths along with the tie stress levels to visualise the load sharing mechanism of ties when the veneer cracked. Fig. 13 shows the tie strength distribution (black column) for all ties at P_{cr} for two representative samples of Type-I (MCS#13) and Type-II (MCS#39) behaviour; however, as a few of the ties (T9 to T12 for Type-I and T11 and T12 for Type-II) from the middle row are in tension at P_{cr}, tensile strengths are reported instead of compression for the easy comparison for these ties. The exact geometric location of the wall ties is shown in Fig. 1 with notations from T1 to T20. The 'red cap' on the stress column (see Fig. 13(b)) represents the post-

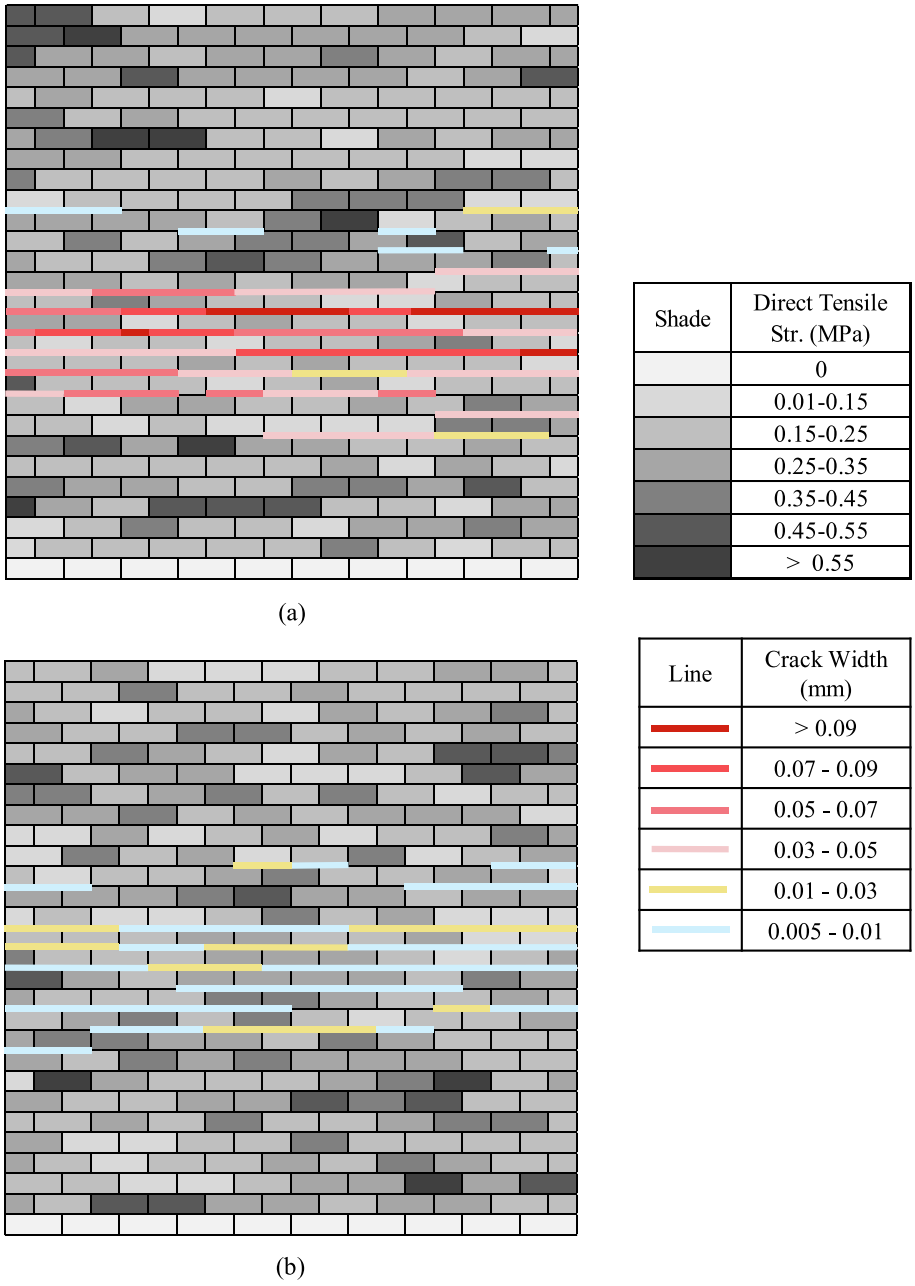

Fig. 11. Cracking pattern and direct tensile strength distribution at P_{cr} for (a) Type-I and (b) Type-II representative FE model.

yielding state, i.e., the unloading stage after reaching the maximum stress level (tie strength). While none of the ties are buckled or failed at P_{cr} for Type-I, six ties (out of eight) from the top two rows are already buckled, and the remaining two are just about to buckle for Type-II.

At the second peak, the total force in ties for the Type-I specimen is greater than for the Type-II. The difference is mostly in the top two rows of ties; for Type-I, the top two rows are still resisting considerable force, whereas for Type-II, the top two rows of ties have moved well along the softening branch (see Fig. 14). All the ties from the top two rows are already yielded, and ties from the bottom row are either yielded or approaching yielding; however, slight differences in behaviour of the middle row of ties (T9 to T12) can be observed between these two types. The Type-I behaviour has a higher second peak because the ties are less damaged at P_{cr} and hence are better able to perform in the load sharing role after veneer cracking compared to the Type-II behaviour. Therefore, the magnitude of the second peak (or system peak) was largely governed by the yielding of the wall ties.

Timber stiffness is a key factor that dictates how the timber-tie connection would deflect when pressure load is transferring from the veneer wall to structural backup (timber) via wall ties. As timber is more flexible than the veneer wall, the deflection capacity of the veneer and timber are not equivalent to each other. The consideration of varying stiffness of the timber studs allows SFEA to incorporate differential deflection, observed from the wall tests [22,23], at a particular row of ties. Moreover, stiffer timber may accelerate the tie buckling compared to that of more flexible timber by providing 'firmer' lateral support to one line of ties compared to other ties in the same veneer wall specimen. However, the actual effect of timber stiffness variability was comprehended from the sensitivity analyses.

4.3.2. *Outward loading*

Fig. 15 represents the pressure vs mid-height wall deflection of 80 MCS under outward loading. A few of the simulations dropped immediately when they peaked at approximately 3.0 kPa with around 5 mm

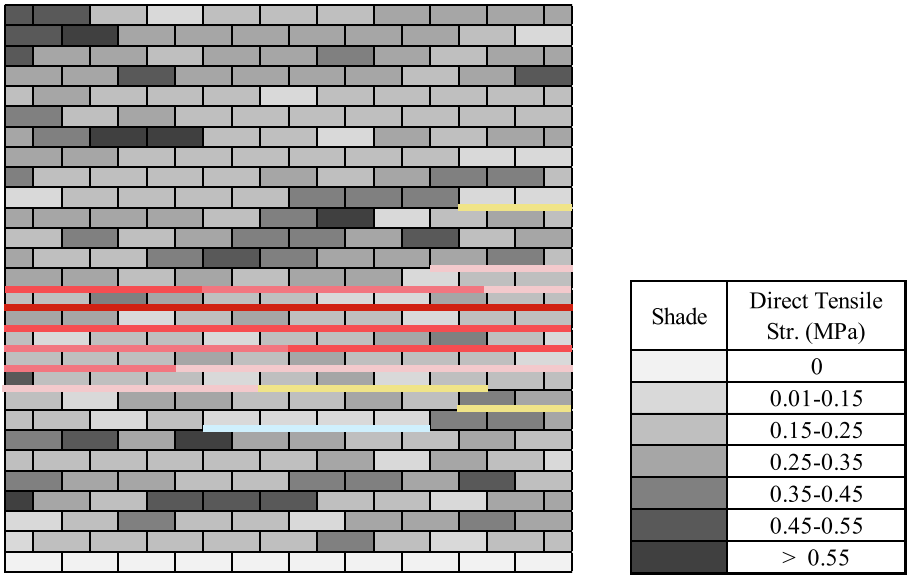

Shade	Direct Tensile Str. (MPa)
	0
	0.01-0.15
	0.15-0.25
	0.25-0.35
	0.35-0.45
	0.45-0.55
	> 0.55

(a)

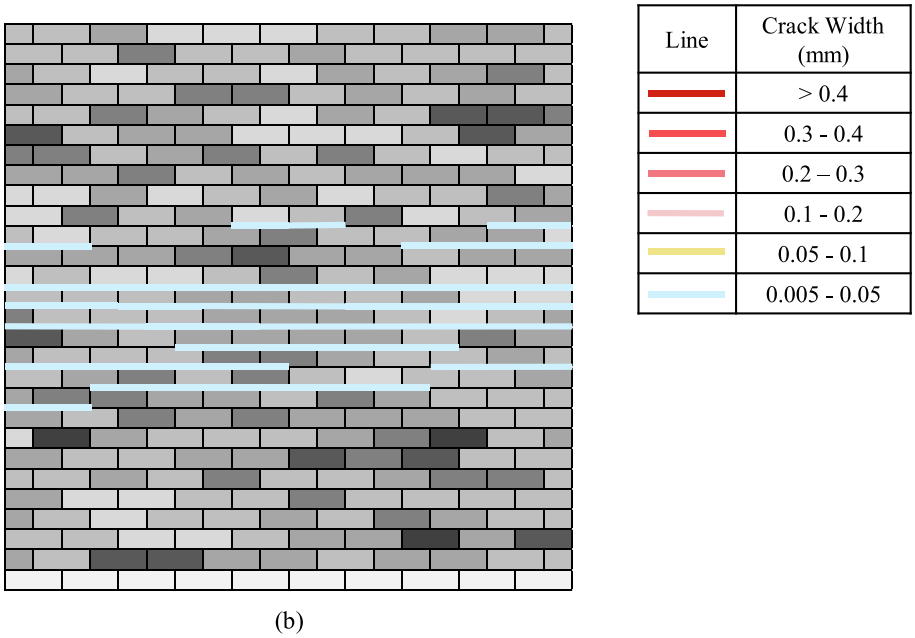

Line	Crack Width (mm)
	> 0.4
	0.3 - 0.4
	0.2 – 0.3
	0.1 - 0.2
	0.05 - 0.1
	0.005 - 0.05

(b)

Fig. 12. Cracking pattern and direct tensile strength distribution at P_{max} for (a) Type-I and (b) Type-II representative FE model.

deflection and failed to converge further in the FEA. The flexural tensile strength was identified as being comparatively higher for those simulations, although it is not conclusive because of the spatially variable f_{mt} for each mortar joint. However, most of the MCS runs had no convergence issues and were able to capture the P_{cr} and P_{max} accordingly. The mean P_{cr} and P_{max} were estimated from the SFEA as 2.2 kPa (COV 0.07) and 3.55 kPa (COV 0.18), respectively.

One representative simulation (one individual realisation) was selected (solid black line in Fig. 15) to examine and explain the failure and tie interaction behaviours of outward SFEA. Fig. 16 depicts the direct tensile strength and veneer cracking distribution of the representative FE model under outward lateral loading. At the mid-height (15 courses), the highest crack widths (interface relative displacement) were observed for P_{cr} along with some minor cracks along the weaker mortar joints. However, cracking widths increased significantly and extend over the wall's surface at P_{max} (see Fig. 16 (b)). For instance, the veneer cracking widths at 14 and 15 courses are just below 1 mm, representing the collapse of the veneer wall due to excessive interface displacement and wall deflection.

Fig. 17 represents the tie stress and strength distributions for all wall ties at P_{cr} and P_{max}. Due to varying tie strength and timber stud stiffness, tie forces for a given row are not equal and tie failure occurs at different stress levels. The observed tie failure pattern (i.e., random) was similar to the wall tests [22,23]. At $P_{cr,}$ only one tie from the top row (T17) is yielded, while the remaining ties exhibited significantly lower stresses than input strengths (see Fig. 17 (a)). This allowed the veneer system to reach a peak load that is notably higher than the deterministic FEA model. At P_{max}, almost all the ties from all rows are about to yield or already yielded; therefore, yielding of wall ties largely governs the magnitude of the system peak load. If the veneer wall cracks prior to yielding of the top row of ties, the wall system has the potential to reach a comparatively higher peak load, as observed for the inward loading SFEA models as well.

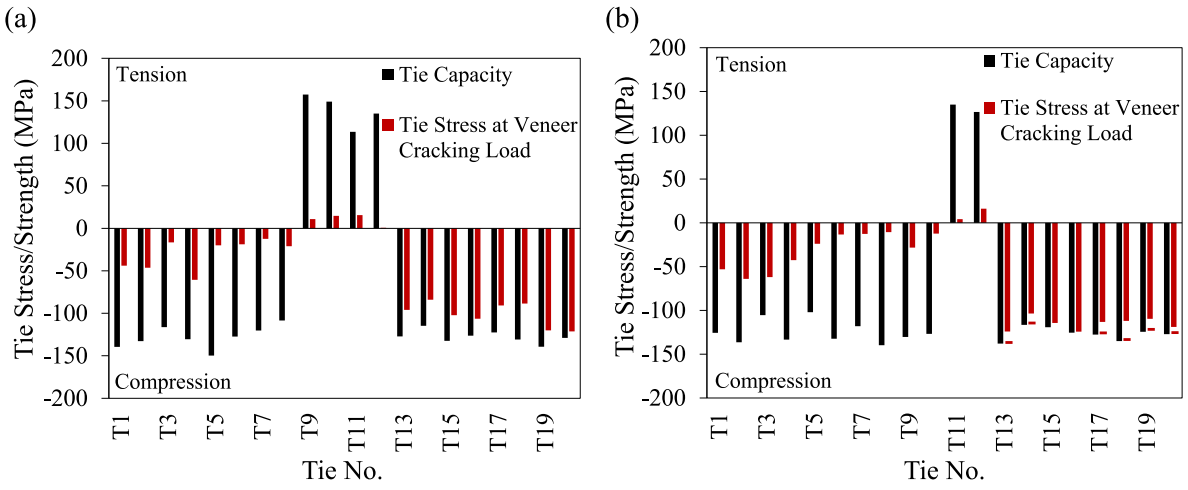

Fig. 13. Tie stress and strength distribution at P_{cr} for (a) Type-I and (b) Type-II representative sample of SFEA.

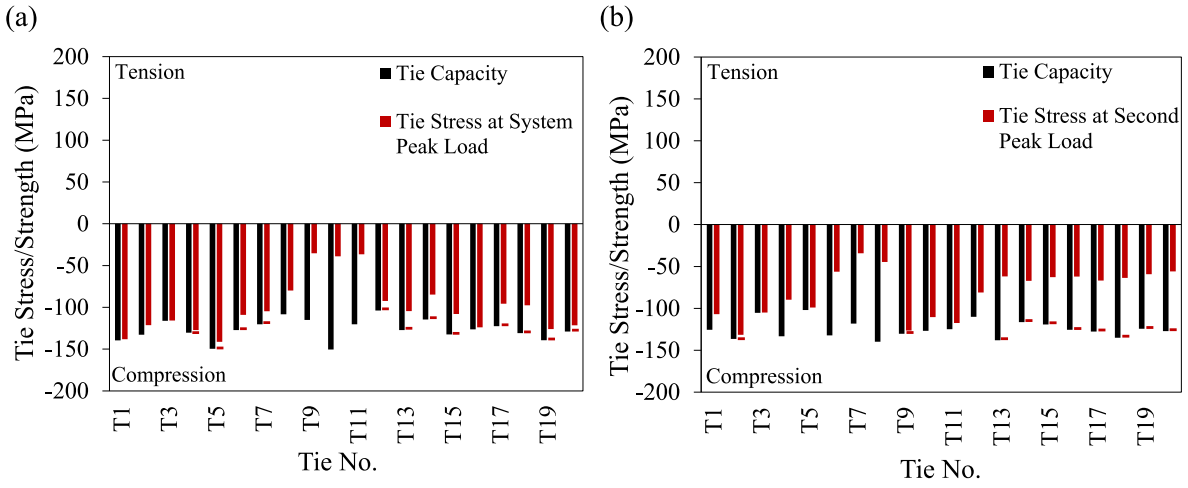

Fig. 14. Tie stress and strength distribution at the (a) system peak (P_{max}) for the Type-I and (b) second peak for the Type-II representative sample of SFEA.

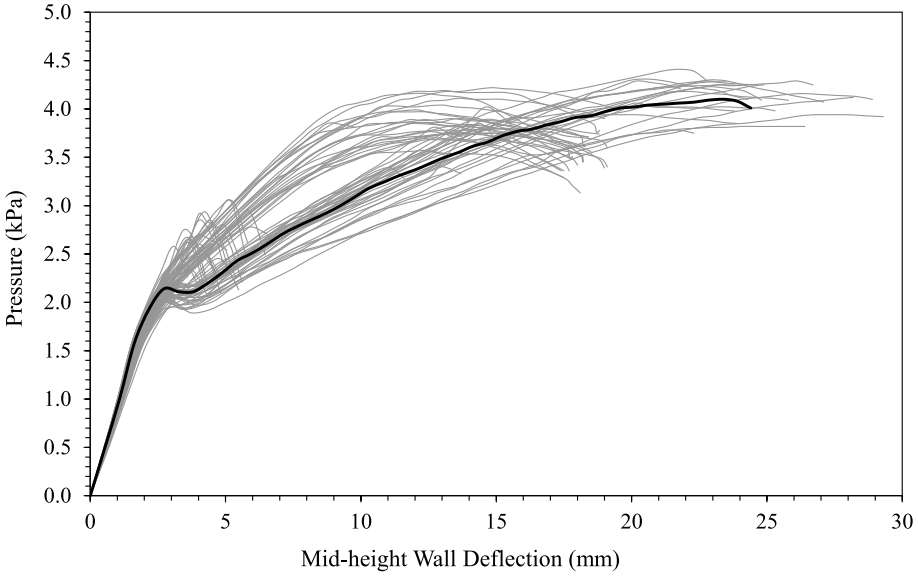

Fig. 15. Pressure load vs deflection plots for 80 MC realisations under outward loading (spatial analysis, ρ = 0.4).

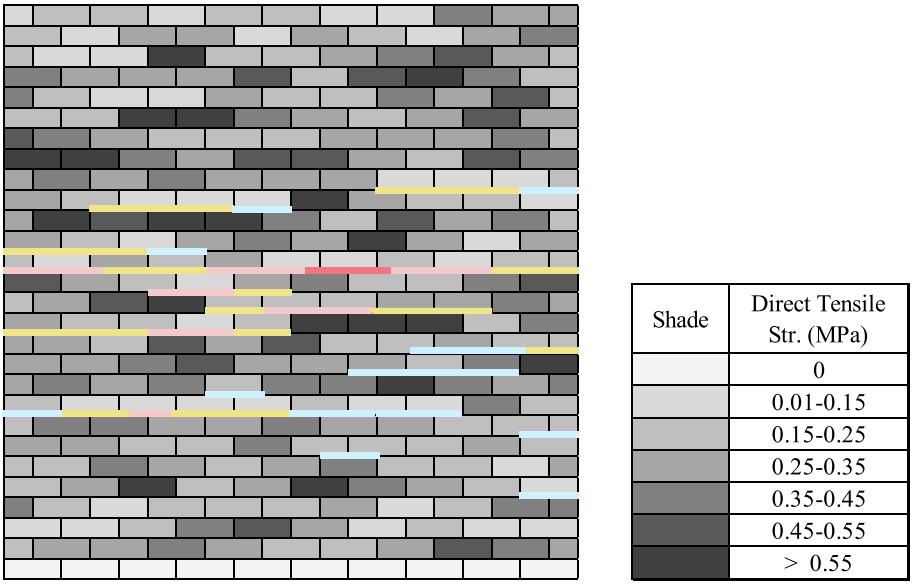

(a)

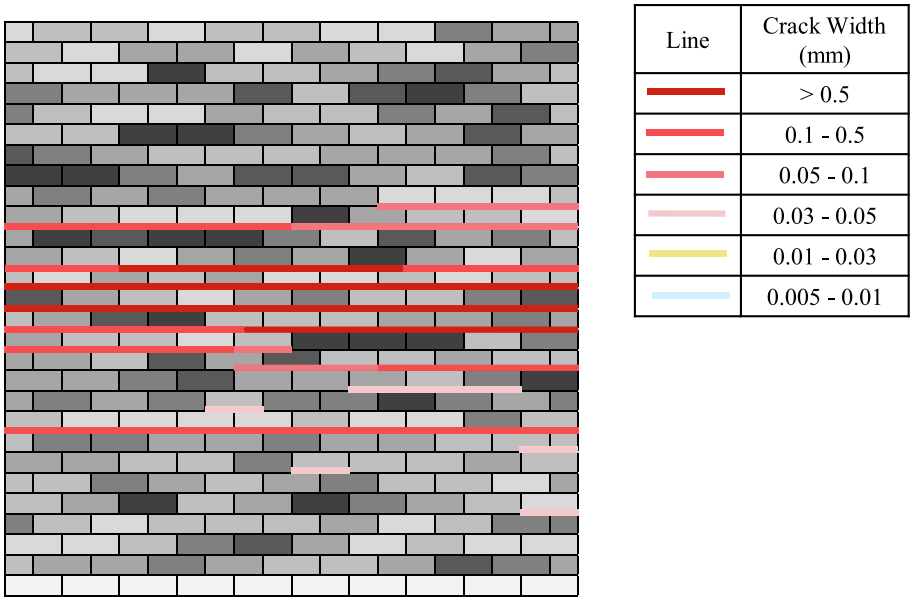

(b)

Fig. 16. Cracking pattern and direct tensile strength distribution at (a) P_{cr} and (b) P_{max} for spatial SFEA under outward loading.

4.4. Spatial analysis with $\rho = 0$

In this case, mortar joints in brick masonry, ties and timber studs properties are treated as statistically independent (i.e., no correlation).

4.4.1. Inward loading

Table 4 shows the mean and COV of P_{cr} and P_{max} and compares them with spatial ($\rho = 0.4$) and non-spatial analyses. For the P_{cr} and P_{max}, the mean values obtained from the spatial analysis with $\rho = 0$ are slightly different, as expected, to those obtained from a spatial analysis with $\rho = 0.4$. Similarly, $\rho = 0$ results in moderately lower COV for both P_{cr} and P_{max} compared to $\rho = 0.4$. The results are explained and compared in detail in section 4.6.

4.4.2. Outward loading

The load–displacement behaviour of 80 MCS runs with $\rho = 0$ is similar to $\rho = 0.4$. Mean P_{cr} and P_{max} for $\rho = 0$ is almost 3.6% lower and 5.6% higher respectively than that of $\rho = 0.4$ (see Table 4). Lower veneer cracking loads lead to a higher system peak load, which was explained in section 4.3. On the other hand, COVs obtained for cracking and system peak loads are comparatively (to $\rho = 0.4$) lower for spatial analysis with $\rho = 0$.

4.5. Non-Spatial analysis ($\rho = 1$)

The non-spatial analysis is the case where all the joints of the masonry veneer wall have the same flexural bond strength and the same tie strength and timber stiffness regardless of their position in the wall for each simulation, i.e., fully correlated and considered homogenous material properties.

4.5.1. Inward loading

Fig. 18 depicts the veneer wall's load vs. mid-height displacement plots for 60 MCS runs under inward loading where no spatial variability

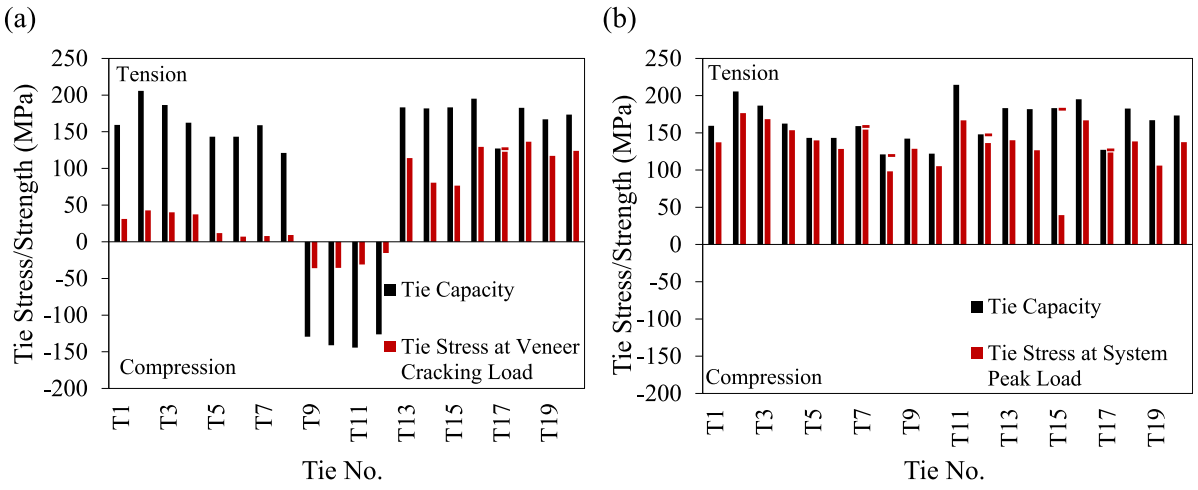

Fig. 17. Tie stress and strength distributions at the (a) P_{cr} and (b) P_{max} for spatial SFEA under outward loading.

Table 4
Summary of spatial and non-spatial analyses.

Loading Category	Sample Size	Analysis	P_{cr}		P_{max}	
			Mean (kPa)	COV	Mean (kPa)	COV
Inward	1	Deterministic	2.53	–	2.53	–
	60	Spatial $\rho = 0$	2.31	0.07	2.72	0.11
	60	Spatial $\rho = 0.4$	2.33	0.09	2.71	0.13
	60	Non-spatial $\rho = 1$	2.13	0.18	2.78	0.18
Outward	1	Deterministic	2.12	–	3.06	–
	80	Spatial $\rho = 0$	2.12	0.04	3.75	0.13
	80	Spatial $\rho = 0.4$	2.20	0.07	3.55	0.18
	80	Non-spatial $\rho = 1$	1.97	0.15	3.70	0.20

is considered. The larger 'scatter' in the behaviour of the load–displacement curves compared to spatial analysis is noticeable, representing the higher variabilities. The non-spatial analysis exhibited the lowest mean value (2.13 kPa) for P_{cr} and the highest mean value (2.78 kPa) for P_{max} compared to any other spatial analyses. Moreover, maximum variabilities (COVs of 18%) for P_{cr} and P_{max} under inward loading are also observed for this analysis compared to any other analyses. The estimated peak load from the non-spatial analysis is 1.8% and 2.6% higher than that estimated from the spatial analysis with $\rho = 0$ and 0.4, respectively. Relatively lower tie stiffness results in significant veneer deflection, which leads the masonry to crack earlier, hence the less stiff behaviour of the overall system, as can be seen from one analysis in Fig. 18.

4.5.2. Outward loading

The Load-displacement plots for 80 MCS runs of non-spatial analysis under outward loading are shown in Fig. 19. Similar to inward loading, non-spatial analysis shows higher variabilities in veneer cracking (P_{cr}) and system peak load (P_{max}) compared to spatial analyses. Mean P_{cr} and P_{max} observed for non-spatial analysis is almost 10.5% lower and 4.2% higher, respectively, than that observed for spatial analysis with $\rho = 0.4$. In comparison to $\rho = 0$, the respective mean values are about 7% and 1.5% lower.

4.6. Comparison of spatial and Non-Spatial analyses

A summary of veneer cracking and system peak loads for non-spatial

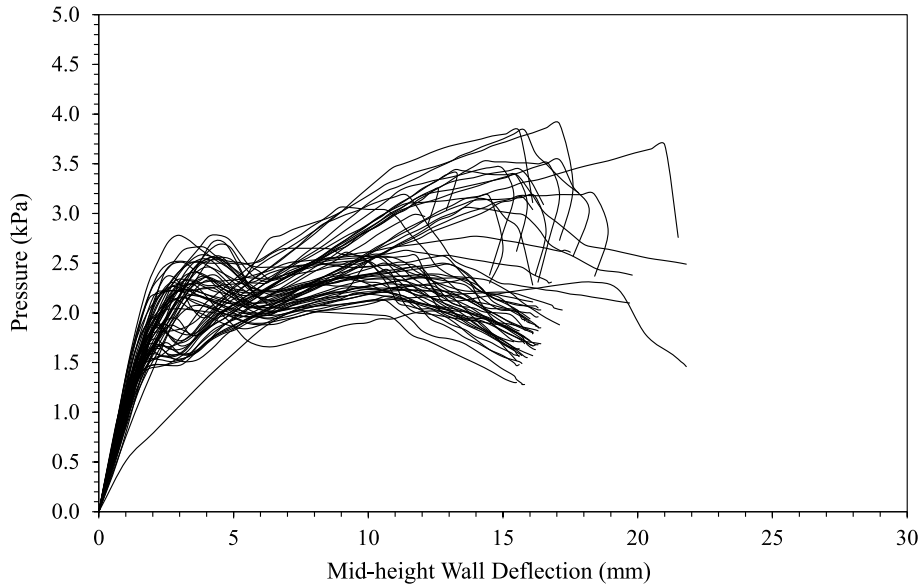

Fig. 18. Pressure load vs deflection plots for 60 MC realisations under inward loading (non-spatial analysis).

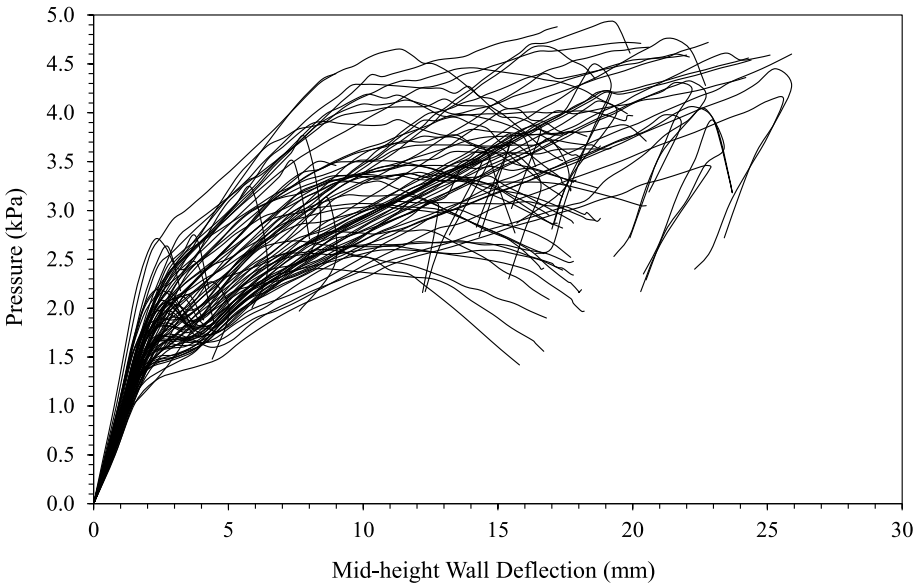

Fig. 19. Pressure load vs deflection plots for 80 MC realisations under outward loading (non-spatial analysis).

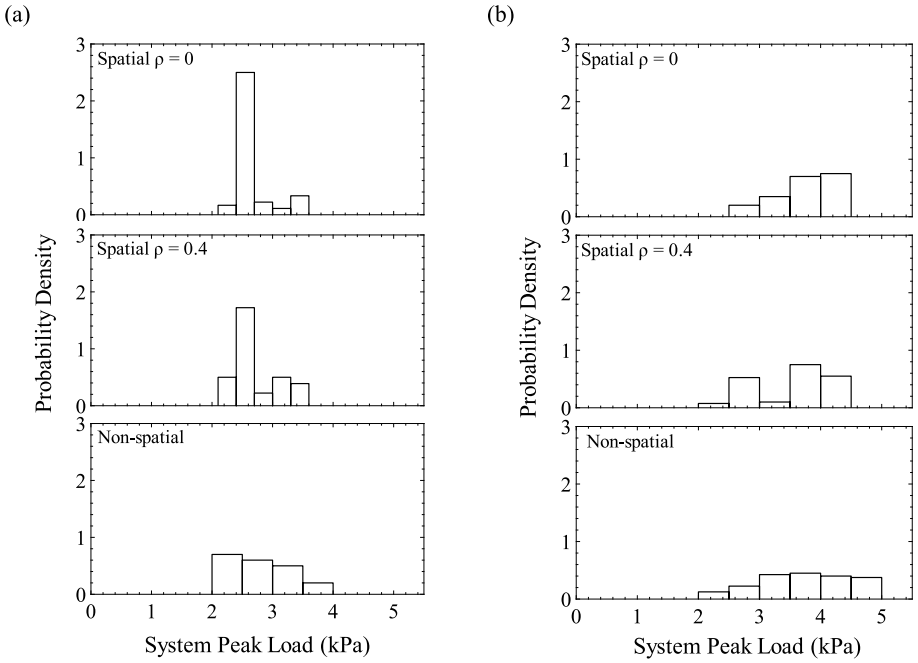

Fig. 20. Simulation histograms of system peak load for (a) inward loading and (b) outward loading.

and spatial analyses under inward and outward out-of-plane loading is compared in Table 4. Moreover, simulation histograms of system peak load from the SFEA for non-spatial and spatial (with $\rho = 0$ and 0.4) analyses under inward and outward loadings are reported in Fig. 20. It can be observed that ignoring spatial variability of the wall system components (unit flexural bond strength, tie strength and timber stiffness) underestimates the system peak load in the lower tail of the simulation histograms for both inward and outward loading. A non-spatial analysis therefore will overestimate the probability of wall failure compared to a spatial analysis.

The system peak load (wall strength) is the load at which wall system components failed (mostly brick veneer and wall ties). Therefore, this may occur at a lower wall pressure load for the spatial case due to the presence of lower than average strength mortar joints and wall ties than in the non-spatial case, for which all units and wall ties have equal strength. For inward loading, spatial analysis with $\rho = 0$ estimates the mean system peak load 2.2% lower than that estimated from the non-spatial analysis. Similarly, for outward loading, this difference (between $\rho = 0$ and non-spatial) is also less pronounced; nevertheless, the non-spatial analysis estimates peak load 4.2% higher in comparison to $\rho = 0.4$. The presence of 'weak' joints randomly located in the wall for spatial analysis may initiate the cracking in the wall earlier (lower pressure level) than the non-spatial analysis in the masonry wall; however, masonry cracking depends on the tie and timber stiffness as well. The load sharing mechanism between mortar joint and wall ties after veneer cracking is complex; thus, it cannot be established with a linear relationship.

Table 4 also illustrates that the COV of the veneer cracking load (P_{cr}) and system peak load (P_{max}) obtained from the spatial analysis with $\rho = 0$ are significantly lower than the COV obtained from the non-spatial

Table 5
Simulation scheme and results of sensitivity analysis.

Loading Type	Notation	Brick Veneer	Wall Ties	Timber Studs	No. of Runs	Peak Load, P_{max}	
						Mean (kPa)	COV
Inward	Deterministic	Det.	Det.	Det.	01	2.53	–
	SFEA ρ = 0.4	Stoc.	Stoc.	Stoc.	60	2.71	0.13
	I_Veneer	Det.	Stoc.	Stoc.	60	2.47	0.03
	I_Tie	Stoc.	Det.	Stoc.	60	2.58	0.06
	I_Timber	Stoc.	Stoc.	Det.	60	2.63	0.13
Outward	Deterministic	Det.	Det.	Det.	01	3.06	–
	SFEA ρ = 0.4	Stoc.	Stoc.	Stoc.	80	3.55	0.18
	O_Veneer	Det.	Stoc.	Stoc.	80	3.32	0.16
	O_Tie	Stoc.	Det.	Stoc.	80	3.01	0.06
	O_Timber	Stoc.	Stoc.	Det.	80	3.45	0.18

Det. = Deterministic; Stoc. = Stochastic

analysis, with the effect being more pronounced for P_{cr}. For every simulation of spatial analysis with ρ = 0, it is always the wall system components (mortar joints, wall ties and timber studs) with strength and/or stiffness values below the mean that influences the P_{cr} and P_{max}. On the other hand, for the non-spatial analysis, the randomly generated wall component strength or stiffness can all be a smaller value or can also all be a larger value than the mean strength. Smaller than average wall component strength values result in a smaller than average veneer cracking load, while larger than average strength values result in a larger than average cracking load, for non-spatial analysis by default. As expected, the system peak load is also affected to a higher degree; hence, the COV in the non-spatial analysis is higher than the spatial analysis.

The load sharing between mortar joints and ties plays a crucial role in reaching the system peak load after the veneer cracked. The probability of a weak joint being surrounded by higher strength joints is highest for the analysis ρ = 0 of the two spatial analysis cases. This distribution of mortar joint strengths may restrict or delay the crack propagation, i.e., pushing the peak load to a later load step. However, relative tie strength and timber stiffness may alter this phenomenon.

The COVs of veneer cracking load for outward loading calculated from both spatial and non-spatial analyses are lower than the COVs obtained for inward loading. For outward loading, the P_{cr} is determined based on the stiffness changes of the load–deflection response for a significant number of MCS runs, unlike inward loading. Hence, fewer variations were possible when capturing veneer cracking loads. However, the principal objective of this study is to estimate the system peak load, i.e., wall system strength (crucial to the design of veneer wall systems) and capture the associated variabilities. The COV of the system peak load for outward loading is higher than inward loading for any given analysis type which is largely a result of the veneer and tie failure mechanism at P_{max}. When the brick veneer cracks, the masonry wall is supported mainly through wall ties. Under outward loading, wall ties experience tensile force and start to deform according to the tie constitutive law. The post-peak tensile behaviour of the wall tie is defined by point D (see Fig. 7), which has a higher COV (49%) compared to compressive post-peak tie behaviour (17% and 33% for points C and D, respectively). The peak and post-peak deformation of wall ties govern the wall system peak load (see section 4.3.2) consequently, higher COV was obtained for the P_{max} under outward loading than the inward loading. Therefore, it can be established that, under outward out-of-plane loading, wall tie properties significantly impact the veneer wall system behaviour.

In summary, a non-spatial analysis will overestimate the probability of wall system failure compared to a spatial analysis; furthermore, the spatial analysis should be considered to better (more realistically) represent the variabilities associated with the URM veneer wall system. Furthermore, Heffler [13] established the unit to unit spatial correlation as ρ = 0.4 from extensive experiments, and Li et al. [14,15] observed that ρ = 0.4 is the most realistic among the spatial simulations. Hence, the sensitivity analysis and model error statistics are discussed in the following sections considering spatial SFEA with ρ = 0.4.

Table 6
Comparison of experimental and spatial SFEA results.

Loading Category	Load	Monte-Carlo Experiments		MC Corrected Peak Load (V_E)		Spatial SFEA (V_M)	
		Mean (kPa)	COV	Mean (kPa)	COV	Mean (kPa)	COV
Inward	P_{max}	2.80	0.11	2.80	0.10	2.71	0.13
Outward	P_{max}	3.68	0.21	3.68	0.19	3.55	0.18

4.7. Sensitivity analysis

A sensitivity analysis study was conducted to evaluate the relative impact of the variability and uncertainty of the SFEA model parameters on the strength prediction of the veneer wall system. This was achieved by running the MCS analysis with each parameter in turn modelled deterministically while all other parameters were modelled probabilistically. A total of three scenarios were considered for each loading type, as shown in Table 5. Each scenario is labelled as < Type of loading>_<Parameter considered as deterministic > .

For inward loading, the peak load (P_{max}) is comparatively more sensitive to veneer wall bond strength and tie strength because when veneer wall bond strength and tie strength were considered as deterministic, the COV of the P_{max} of the whole veneer system drops significantly, i.e., unable to sufficiently capture the variability of the system. On the other hand, when timber stiffness is considered deterministic, the COV of the peak load is unaffected.

For outward loading, P_{max} appeared to be the most sensitive to tie strength variability. Similar to inward loading, the veneer system peak load is less sensitive to timber stiffness variability.

5. Comparison of mc experimental and sfea results

A direct comparison between Monte-Carlo (MC) experimental and stochastic FEA results is not the 'accurate' representation of the FE model's efficiency. A COV obtained from the wall tests may overestimate the true variations of wall failure load (P_{max}) due to (i) the accuracy of the test measurements and definitions of failure, and (ii) differences between the strengths of the test specimen (full-scale veneer wall systems) and control specimens (e.g., bond-wrench prisms). Muhit et al. [22] factored out these uncertainties from the experimental COV to make it comparable with SFEA. Hence, the corrected COV (V_E) for inward and outward loading was estimated to be 0.10 and 0.19, respectively. The comparison summary between Monte-Carlo experimental and spatial SFEA results (ρ = 0.4) in terms of the veneer system's peak load is given in Table 6.

In terms of wall system failure load, spatial SFEA underestimated the experimental mean by 3.2% and 3.5% for inward and outward loading,

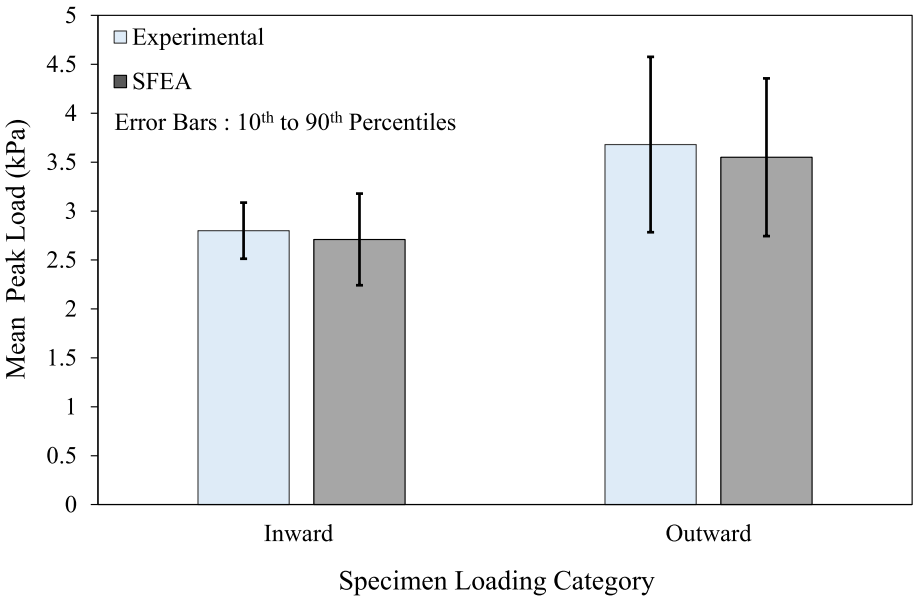

Fig. 21. Comparison of mean peak experimental and SFEA results for inward and outward loading.

respectively. On the other hand, for inward loading, the COV of SFEA is higher (0.13) than the Monte-Carlo corrected experimental results (0.10), which might be due to the two distinct load–displacement behaviours (second-peak $> P_{cr}$ and second-peak $\leq P_{cr}$) recorded in the SFEA, while in the experiment (wall tests) only the second-peak $> P_{cr}$ scenario was observed, as explained in section 4.3.1. It is unexpected for MC experimental results to have a lower COV than SFEA. However, the COV of SFEA is quite close (0.18) to experimental results (0.19) for the outward loading category. For each loading category, the mean system peak load (P_{max}) from the spatial SFEA are compared with experimental results in Fig. 21.

It is crucial to know if the test results could be considered part of the same population as the spatial SFEA. Therefore, a hypothesis testing, Student's *t*-test, is conducted for both inward and outward loading categories. The null hypothesis that these results came from the same population was not rejected at a 95% confidence interval for inward (t-score = 0.7084 and p = 0.4824) and outward (t-score = 0.5482 and p = 0.5850) loading categories. By conventional criteria, the above-mentioned t-scores and the two-tailed p-values indicate that the difference between experimental and SFEA results is not statistically significant, i.e., the SFEA and experimental results can be considered to be from the same population for both inward and outward loading categories. A similar finding occurs if the Z-test is used.

6. Model error

Every model may have some level of error and uncertainty in its predictive capacity. The model error (*ME*) is defined as the ratio between experimental capacity and predicted capacity from the SFEA, expressed as:

$$ME = \frac{ExperimentalCapacity}{ModelPredictedCapacity} \tag{5}$$

The respective inward and outward loading mean model errors are calculated as 2.80/2.71 = 1.03 and 3.68/3.55 = 1.04, respectively. Model error close to '1' indicates an accurate model prediction and in this case, the SFEA accurately predicts mean capacity. It is noteworthy that as the COV of the 'experimental capacity' of equation (5) is calculated based on the variability of the test procedures and the specimen variability, it represents more than just the model's accuracy. For outward loading, V_E is very close to the COV of the SFEA. On the contrary, the COV of the SFEA is slightly greater than that of experimental results for inward loading. These results indicate that the spatial SFEA models sufficiently represents the variability of the experimental results. The Student's *t*-test and Z-test also confirmed that results from the experimental programme and SFEA came from similar populations. Hence, it may be assumed that the variability of model error can be considered as zero in future studies (e.g., reliability analysis).

7. Conclusions

A computational method and probabilistic model have been developed to estimate the strength of unreinforced masonry veneer wall systems subjected to inward and outward out-of-plane loading. The spatial SFEA model considered the spatial variability (unit to unit correlation $\rho = 0$ and 0.4) of the wall components (mortar flexural tensile strength, wall tie strength/stiffness and timber stud stiffness) and compared them with non-spatial analysis.

The non-spatial analysis seems to overestimate the wall system failure compared to spatial analysis; furthermore, the spatial analysis is considered to represent the variabilities of the URM veneer wall system realistically.

A sensitivity analysis found that timber stiffness variability has less influence on the response for both loading directions while tie strength variability exhibited a significant effect on wall system failure.

This paper emphasises the importance of spatial SFEA to accurately capture the material variabilities and estimate the system peak load capacity. From the comparison of laboratory wall testing and SFEA results, it is evident that the stochastic finite element model developed in this study is able to estimate the behaviour and system peak load reasonably and are considered to be from the similar population as test results.

CRediT authorship contribution statement

Imrose B. Muhit: Methodology, Software, Validation, Formal analysis, Investigation, Data curation, Writing – original draft, Writing – review & editing, Visualization. **Mark J. Masia:** Conceptualization, Investigation, Resources, Writing – review & editing, Supervision, Funding acquisition. **Mark G. Stewart:** Conceptualization, Methodology, Writing – review & editing, Supervision, Project administration, Funding acquisition. **Andrea C. Isfeld:** Software, Investigation, Writing

– review & editing.

Declaration of Competing Interest

The authors declare that they have no known competing financial interests or personal relationships that could have appeared to influence the work reported in this paper.

Acknowledgements

The authors wish to acknowledge the financial support of the Australian Research Council under Discovery Project DP180102334.

References

[1] Standards Australia. (2018). Masonry Structures (AS 3700:2018). Standards Australia Limited, Australia.
[2] Lawrence, S. J. and Lu, J. P. (1991). An elastic analysis of laterally loaded masonry walls with openings. Proceedings of the International Symposium on Computer Methods in Structural Masonry, Swansea, UK.
[3] Page AW, Kautto J, Kleeman PW. A Design Procedure for Cavity and Veneer Wall Ties. Masonry International 1996;10(2):55–62.
[4] Yi J, Laird D, McEwen B, Shrive NG. Analysis of load in ties in masonry veneer walls. Can J Civ Eng 2003;30(5):850–60.
[5] Okail, H. (2010). *Experimental and Analytical Investigation of the Seismic Performance of Low-Rise Masonry Veneer Buildings* [PhD Thesis, University of California, San Diego]. University of California Research Repository.
[6] Jo, S. (2010). *Seismic Behavior and Design of Low-rise Reinforced Concrete Masonry with Clay Masonry Veneer* [PhD Thesis, The University of Texas at Austin]. The University of Texas Repository.
[7] Reneckis D, LaFave JM. Out-of-plane seismic performance and detailing of Brick Veneer walls. J Struct Eng 2010;136(7):781–93.
[8] Malomo D, Pinho R, Penna A. Numerical modelling of the out-of-plane response of full-scale brick masonry prototypes subjected to incremental dynamic shake-table tests. Eng Struct 2020;209.
[9] Baker LR. Variation in flexural strength of brickwork with beam span and loading. J. Australian Ceramic Soc. 1974;10(2):25–38.
[10] Lawrence, S. J. and Cao, H. T. (1988). Cracking of non-loadbearing masonry walls under lateral forces. *Proceedings of the 8th International Brick Masonry Conference*, Dublin, Ireland.
[11] Lawrence, S. J. (1991). Stochastic analysis of masonry structures. *Proceedings of the International Symposium on Computer Methods in Structural Masonry*, Swansea, UK.
[12] Stewart MG, Lawrence SJ. Structural reliability of masonry walls in flexure. Masonry International 2002;15(2):48–52.
[13] Heffler, L. M. (2009). *Variability of Unit Flexural Bond Strength and its Effect on Strength in Clay Brick Unreinforced Masonry Walls Subject to Vertical Bending* [MPhil Thesis, The University of Newcastle, Australia]. The University of Newcastle Research Repository.
[14] Li J, Masia MJ, Stewart MG, Lawrence SJ. Spatial variability and stochastic strength prediction of unreinforced masonry walls in vertical bending. Eng Struct 2014;59:787–97.
[15] Li J, Stewart MG, Masia MJ, Lawrence SJ. Spatial Correlation of Material Properties and Structural Strength of Masonry in Horizontal Bending. J Struct Eng 2016;142(11):04016112.
[16] Li J, Masia MJ, Stewart MG. Stochastic spatial modelling of material properties and structural strength of unreinforced masonry in two-way bending. Struct Infrastruct Eng 2016;13(6):683–95.
[17] Doherty, K. T. (2000). *An Investigation of the Weak Links in the Seismic Load Path of Unreinforced Masonry Buildings* [PhD Thesis, Department of Civil and Environmental Engineering, The University of Adelaide]. The University of Adelaide Research Repository.
[18] Isfeld AC, Stewart MG, Masia MJ. Stochastic finite element model assessing length effect for unreinforced masonry walls subjected to one-way vertical bending under out-of-plane loading. Eng Struct 2021;236.
[19] Baker, L. R. (1981). *Flexural action of masonry structures under lateral load* [PhD Thesis, School of Engineering and Architecture, Deakin University], Deakin University Library.
[20] Vaculik J, Griffith MC. Probabilistic Analysis of Unreinforced Brick Masonry Walls Subjected to Horizontal Bending. J Eng Mech 2017;143(8):04017056.
[21] Müller D, Förster V, Graubner C-A. Influence of material spatial variability on required safety factors for masonry walls in compression. Mauerwerk 2017;21(4):209–22.
[22] Muhit IB, Masia MJ, Stewart MG. Monte-Carlo laboratory testing of unreinforced masonry veneer wall system under out-of-plane loading. Constr Build Mater 2022;321.
[23] Muhit, I. B. (2021). Stochastic Assessment of Unreinforced Masonry Veneer Wall Systems Subjected to Lateral Out-of-Plane Loading [PhD Thesis, The University of Newcastle, Australia]. The University of Newcastle Research Repository. Identifier: http://hdl.handle.net/1959.13/1428806.
[24] Standards Australia. (2015). *Masonry in small buildings – Construction* (AS 4773.2: 2015), Standards Australia Limited, Australia.
[25] DIANA FEA BV. (2019). *DIANA - Finite Element Analysis*, User's Manual release 10.3. Delft, The Netherlands.
[26] Lourenco, P. B. (1996). *Computational strategies for masonry structures* [PhD Thesis, Delft University of Technology, Netherlands. TU Delft Research Library.
[27] Lourenço PB, Rots JG, Blaauwendraad J. Two approaches for the analysis of masonry structures: micro and macro-modelling. HERON 1995;40(4):313–40.
[28] Lourenco PB, Rots JG. Multisurface interface model for analysis of masonry structures. J Eng Mech 1997;123(7):660–8.
[29] Muhit IB, Stewart MG, Masia MJ. Probabilistic constitutive law for masonry veneer wall ties. Aust J Struct Eng 2022;23(2):97–118.
[30] Lourenco, P. B. (2008). Structural masonry analysis: Recent developments and prospects. *Proceedings of the 14th International Brick and Block Masonry Conference*, Sydney, Australia.
[31] Van der Pluijm R. Non-linear behaviour of masonry under tension. Heron 1997;42(1):25–54.
[32] Petersen, R. B. (2009). *In-plane Shear Behaviour of Unreinforced Masonry Panels Strengthened with Fibre Reinforced Polymer Strips* [PhD Thesis, The University of Newcastle, Australia]. The University of Newcastle Research Repository.
[33] Gooch LJ, Masia MJ, Stewart MG. Application of stochastic numerical analyses in the assessment of spatially variable unreinforced masonry walls subjected to in-plane shear loading. Eng Struct 2021;235.
[34] Raphael JM. Tensile Strength of Concrete. ACI Journal 1984;81(2):158–65.
[35] Masia, M. J., Simundic, G., and Page, A. W. (2012). Assessment of the AS3700 relationship between shear bond strength and flexural tensile bond strength in unreinforced masonry. *Proceedings of the 15th International Brick and Block Masonry Conference*, Florianopolis, Brazil.
[36] Milani G, Lourenco PB. Simple Homogenized Model for the Nonlinear Analysis of FRP Strengthened Masonry Structures. II: Structural Applications. J Eng Mech 2013;139(1):77–93.
[37] Correa MRS, Masia MJ, Stewart MG, Heffler LM. An Experimental and Statistical Analysis of the Flexural Bond Strength of Masonry Walls. Aust J Struct Eng 2012;13(2):139–48.
[38] MathWorks Inc. (2018). MATLAB, MathWorks, Natick, Massachusetts.
[39] Milani G, Benasciutti D. Homogenized Limit Analysis of Masonry Structures with Random Input Properties: Polynomial Response Surface Approximations and Monte Carlo Simulations. Structural Engineering and Mechanics 2010;34(4):417–47.